

AD-A251 673




**DEPARTMENT OF DEFENCE
DEFENCE SCIENCE AND TECHNOLOGY ORGANISATION
AERONAUTICAL RESEARCH LABORATORY**

MELBOURNE, VICTORIA

Flight Mechanics Report 189

DTIC
ELECTE
JUN 22 1992
S A D

**VISUALISATION IN WATER OF VORTEX FLOW
OVER SHARP-EDGED CANARD CONFIGURATIONS**

by

D.H. THOMPSON

92-16345


This document has been approved
for public release and sale; its
distribution is unlimited.

Approved for public release.

© COMMONWEALTH OF AUSTRALIA 1992

APRIL 1992

92 6 19 058

This work is copyright. Apart from any fair dealing for the purpose of study, research, criticism or review, as permitted under the Copyright Act, no part may be reproduced by any process without written permission. Copyright is the responsibility of the Director Publishing and Marketing, AGPS. Enquiries should be directed to the Manager, AGPS Press, Australian Government Publishing Service, GPO Box 84, CANBERRA ACT 2601.

**DEPARTMENT OF DEFENCE
DEFENCE SCIENCE AND TECHNOLOGY ORGANISATION
AERONAUTICAL RESEARCH LABORATORY**

Flight Mechanics Report 189

**VISUALISATION IN WATER OF VORTEX FLOW
OVER SHARP-EDGED CANARD CONFIGURATIONS**

by

D.H. THOMPSON

SUMMARY



A wing/canard configuration with sharp, highly swept leading edges was tested in a small towing tank. Flow visualisation techniques were used to study the effects of canard position on vortex interactions and vortex breakdown. A canard above or co-planar with the wing delayed wing vortex breakdown. A canard below the wing produced a strong interaction between the wing and canard vortices and could cause early wing vortex breakdown. Depending on its longitudinal position, the low canard could seriously disrupt the wing flow.



© COMMONWEALTH OF AUSTRALIA 1992

POSTAL ADDRESS: Director, Aeronautical Research Laboratory
506 Lorimer Street, Fishermens Bend 3207
Victoria Australia

Accession For	
NTIS CRA&I	<input checked="" type="checkbox"/>
DTIC TAB	<input type="checkbox"/>
Unannounced	<input type="checkbox"/>
Justification	
By	
Distribution /	
Availability Codes	
Dist	Avail and/or Special
A-1	

CONTENTS

1. INTRODUCTION	1
2. EXPERIMENTAL TECHNIQUES	2
2.1 Test Facilities	2
2.2 Models	2
2.3 Flow Visualisation Techniques	3
2.4 Test Conditions	3
3. RESULTS AND DISCUSSION	3
3.1 General Flow Features	3
3.2 Effects of Incidence	4
3.2.1 Low-canard configuration	
3.2.2 High-canard configuration	
3.2.3 Mid-canard configuration	
3.3 Effect of Canard Longitudinal Position	7
3.3.1 Low-canard configuration	
3.3.2 High-canard configuration	
3.3.3 Mid-canard configuration	
3.4 Effect of Canard Vertical Position	9
3.5 Flow near Wing Apex	9
3.6 Effect of Canard on Vortex Breakdown	10
4. CONCLUSIONS	11
REFERENCES	
FIGURES	
DISTRIBUTION	
DOCUMENT CONTROL DATA	

VISUALISATION IN WATER OF THE VORTEX FLOW OVER SHARP-EDGED CANARD CONFIGURATIONS

1. INTRODUCTION

In the aerodynamic design of an aircraft, a canard, or tail-first, layout can offer some potential performance advantages over a conventional, rear-tail layout. In the case of a stable aircraft in trimmed flight, a rear tail usually carries a download, and this download must be countered by additional upload produced by the wing. On the other hand, a canard or foreplane will carry an upload for trimmed flight, thus contributing, with the wing, to the overall lift of the aircraft. However, consideration of other factors in aircraft design¹ has meant that relatively few canard configurations have gone into production.

For an aircraft which is basically unstable, as are several modern combat designs, a canard layout can offer distinct advantages, although again the particular details of the aircraft mission can influence the layout choice². The canard layout is a feature of a number of current and proposed designs such as the Saab Viggen and Gripen, the IAI Lavi, and the Eurofighter.

A critical feature of all canard designs, particularly those that are close-coupled, is the way in which the canard and wing flowfields influence each other. The improved efficiency of which canard configurations are capable can be achieved in practice only by proper relative positioning of the lifting surfaces. Numerous studies, both theoretical and experimental, have been undertaken to investigate the effects of layout geometry on the performance of canard configurations^{3,4,5,6}.

Lifting surfaces with sharp, highly-swept leading edges produce strong separated vortex flows at moderate to high angles of attack. When canard configurations employ such lifting surfaces, there are likely to be complex interactions between the vortex systems generated by the wing and canard. Under these circumstances, the determination of the appropriate relative positions of the surfaces is even more critical than in the case of more conventional surfaces, with essentially attached flows.

Behrbohm⁷ carried out a detailed examination of the aerodynamics of a close-coupled canard configuration of small aspect ratio. He showed that it was possible to combine the overall slenderness required for a high-speed aircraft design with the high-lift low-speed capability needed for short-field operations, by making use of favourable vortex interference. Such a configuration was ultimately adopted for the Saab Viggen fighter aircraft⁸.

Calarese⁹ conducted detailed tests in different wind tunnels on a close-coupled canard configuration consisting of a delta-planform canard and a sweptback wing. Velocity fields were surveyed using hot-wire and laser-Doppler anemometry, and flow visualisation studies were carried out. Calarese found that the presence of the canard improved the lift-drag ratio compared to the wing alone.

Hummel and Oelker¹⁰ conducted wind tunnel tests of close-coupled delta wing / delta canard configurations, with sharp, highly-swept leading edges. These tests included surface pressure measurements, surface flow visualisation, total pressure surveys, and force and moment measurements. Some water tunnel flow visualisation tests were carried out also.

Er-EI and Seginer¹¹ conducted schlieren flow visualisation tests on a delta wing / canard configuration in a wind tunnel, and also made force and moment measurements. This work later was extended¹² to include surface pressure measurements.

The objective of the tests described in this report was to determine, using flow visualisation techniques, the structure of the interacting vortex system generated by a close-coupled combination of a canard and a wing, both of which have highly swept leading edges. The effects of varying the relative positions of the canard and the wing, over a range of angles of attack, were examined. Water was used as the working medium and the flow visualisation technique provided a ready means of

determining the position of the vortex cores. The technique also allowed the identification of the location of vortex breakdown in any of the vortices.

2. EXPERIMENTAL TECHNIQUE

2.1 Test Facilities

The experiments were carried using the small towing tank in the Flight Mechanics Branch of the Aeronautical Research Laboratory. This tank is shown schematically in Fig.1. It has a 300 mm square cross-section, and is 6 m long. It is constructed of Perspex, and rests on two parallel steel beams, running lengthwise beneath the tank and supported by pillars at each end.

The towing carriage consists of an aluminium baseplate carried on cylindrical linear bearings running on circular-section steel shafts. The bearing shafts are mounted on steel beams which are positioned beneath the tank support beams, and are supported at either end and at two intermediate positions. This arrangement allows the carriage bearing shafts to be set straight and level, irrespective of the deflection of the tank support beams when the tank is filled with water.

A gantry structure mounted on the carriage baseplate straddles the tank. The gantry is made up of interchangeable sections of aluminium channel and angle, and allows considerable flexibility in the mounting of cameras and lights anywhere above, below, or on either side of the tank.

The carriage is towed by a continuous Kevlar cable, running over a pulley at each end of the tank support structure. One of the pulley shafts is connected by a belt drive to a gearbox, which in turn is connected by a flexible coupling to a variable-speed D.C. electric motor. The carriage velocity is measured using an optical transducer driven by a small trailing wheel mounted on the carriage. The output from the transducer is fed to a microprocessor system which controls the D.C. motor. The microprocessor system allows the user to specify a carriage velocity, or a Reynolds number (for a selected model size). The system controls the carriage acceleration, maintains the required velocity along the tank, and controls deceleration and stopping. The speed range available, depending on the drive pulley installed, is from 0.05 m/s to more than 1.0 m/s.

2.2 Models

The models used in the experiments consisted of a delta wing with a 60° leading edge sweep, and a canard, also of delta planform, with a 70° leading edge sweep. The wing centreline chord (c) was 150 mm and the canard centreline chord was 75 mm. Both models were made from 2 mm thick Perspex sheet, and all edges were symmetrically bevelled to give a 30° included edge angle.

The models were mounted independently on a single sting. Using sliders and spacers, the canard could be positioned in the wing plane ($h/c = 0$), 0.1c above the wing plane ($h/c = +0.1$), or 0.1c below ($h/c = -0.1$). Parallel to the wing plane, the canard could be positioned with its trailing edge up to 0.2c forward of the wing apex ($l/c = -0.2$), or behind the wing apex ($l/c = +0.2$), except in the coplanar case. The range of test positions is shown in Fig.2.

The sting was attached at right angles to a strut which passed up through the water surface to a mounting on the towing carriage gantry. This two-axis mounting allowed the model incidence and yaw to be adjusted. This type of mounting was chosen for simplicity of manufacture, and also because it provided a clear view of the model for photography through the undisturbed water surface. However, it was somewhat inconvenient to use in that each change in model incidence also required adjustment of the strut position in its mounting, and adjustment of the position of the mounting on the carriage, to keep the model in the correct position in the tank. Nevertheless, with practice, the adjustments were performed quickly and easily.

2.3 Flow Visualisation Technique

The hydrogen bubble technique^{14,15}, involving the electrolysis of water, was used to make the flow patterns visible. The cathodes consisted of strips of aluminium foil, 2 mm wide, cemented beneath the leading edges of the wing and canard. A suitable set of metal anodes were positioned in the towing tank. When a voltage was applied between the electrodes, fine bubbles of hydrogen gas formed on the foil strips and were swept off into the vortex systems above the canard and wing. The technique is particularly useful for determining vortex core trajectories, as the low density bubbles are readily carried into the vortex cores and serve to delineate them quite clearly. To promote bubble formation, sodium sulphate was added to the tank water at a concentration of 0.1 g/l.

The bubble patterns were illuminated using 150 W spotlights. For plan view photography, the camera was located on top of the towing carriage gantry, pointing down into the water. A spotlight was mounted on each side of the gantry, slightly below the model, and with its beam angled upwards on to the bubbles.

For side view photography, the camera was mounted on one side of the carriage gantry, pointing in through the side of the tank. A single spotlight was mounted on top of the gantry, offset to the side of the gantry opposite the camera and pointing down into the water at an angle to the camera axis.

Flow patterns were recorded on videotape using a Philips LDH 26 monochrome video camera, and on film using an Olympus OM-2N 35 mm single-lens reflex camera. The film used was Ilford HP5, rated at 1200 ASA, and developed in Microphen.

2.4 Test Conditions

The models were tested over an incidence range from 0° to 30°. The Reynolds number, based on wing centreline chord, was maintained at approximately 100,000, as earlier tests¹⁶ had shown what appeared to be significant Reynolds number effects on interacting vortex patterns above double-delta wings, particularly for Reynolds numbers below 20,000. The incidence setting of the canard was the same as that for the wing for all the tests, that is, the canard plane and the wing plane were parallel. The yaw angle was zero for each test.

Three photographs were taken during each run of the towing carriage along the tank, to check for any variations in vortex pattern during a run. Because the visibility of the hydrogen bubbles was sensitive to the direction of lighting and viewing, it was not possible to take simultaneous plan view and side view photographs during a run, and so photographs from the two viewpoints had to be taken on different runs.

3. RESULTS AND DISCUSSION

3.1 General Flow Features

As a basis for more detailed discussions, the general features of the vortex flow around the wing and canard are described here, taking as examples a configuration with the canard below the plane of the wing, and a configuration with the canard above the plane of the wing. Figs.3 and 4 show a plan view and a side view respectively of the flow around a low-canard configuration ($h/c = -0.1$), with the canard ahead of the wing apex ($l/c = -0.1$). The incidence is 25°.

As with a normal delta wing, a vortex forms above each lateral half of the canard. The vortex originates at the apex of the canard and is formed by the rolling up of the vortex sheet shed by the canard leading edge. The vortex passes downstream over the canard trailing edge, is deflected upwards in the upwash ahead of the wing, and comes under the influence of the vortex system above the wing. A vortex, of the same sense as the canard vortex, forms above and inboard of each wing leading edge, and causes the canard vortex initially to move upwards, then to move down towards the wing surface, and also to move outboard beneath the wing vortex. At the same time, the wing vortex is deflected

inboard and upwards by the canard vortex. The canard and wing vortices thus tend to roll round each other, rotating in a clockwise direction when viewed from downstream (for the vortices above the left-hand side of the wing) and in a counterclockwise direction (for the vortices above the right-hand side).

As can be seen in Fig.3, bursting occurs in each of the canard and wing vortices above the wing, at about 80% of the wing chord. Downstream of the bursts, the flowfield is unsteady and the separate structures of the individual vortices are no longer discernible.

The wing vortices do not originate at the wing apex. Instead, each vortex starts at a point on the leading edge at a chordwise distance from the apex of about 15% of the centreline chord. This shift is due to the velocity field of the canard vortex. The downwash and sidewash inboard of the canard vortex core are such as to reduce the local incidence and/or sweepback of the wing leading edge to a point where vortex formation above the wing does not occur. Outboard of the canard vortex core, the upwash and sidewash effects are such as to promote the formation of a leading-edge vortex.

The effect of the canard on the point of origin of the wing vortex was suggested by Behrbohm⁷. Hummel and Oelker¹⁰ also found similar effects using surface flow visualisation techniques in their wind tunnel experiments. This particular flow feature is discussed in more detail in Section 3.5 of this Report.

Figs.5 and 6 show respectively a plan view and a side view of the flow round a high canard configuration ($h/c = 0.1$), with the canard ahead of the wing apex ($l/c = -0.1$) and again at an incidence of 25° .

As with the low canard configuration, two vortices originate at the apex of the canard and pass downstream over the trailing edge of the canard. However, because of the greater separation between the wing and canard vortices, the effect of the wing vortex system on each canard vortex is less pronounced than is the case with the low canard configuration. The canard vortex which, in the absence of the wing, would align itself at a slight downward inclination to the freestream direction, is deflected downwards just downstream of the wing apex, under the influence of the wing vortex system. The canard vortex also is deflected inboard at about the same chordwise station. In this case, the interaction between the vortex systems is not sufficiently pronounced to cause the canard and wing vortices to intertwine and merge above the wing. The wing vortex streams straight back from the apex with no discernible deflection.

The influence of the canard vortex on the local flowfield near the wing apex is not sufficient to suppress separation at the leading edge or to displace the wing vortex point of origin outboard along the leading edge, as occurs with the low canard. In this case, the wing vortices originate at the wing apex.

The wing vortices burst at about 65-70% of the wing chord, slightly upstream of the corresponding position for the low canard configuration. The situation with the canard vortices is less certain. At about 70-80% of the wing chord, the canard vortex cores undergo an expansion in diameter, but the expansion is less abrupt than is the case for the wing vortices. The core structure downstream of the expansion is unsteady, and although differing in appearance from the wing vortex burst, the overall characteristics of the canard vortex expansion seem to indicate that some form of burst has occurred.

3.2 Effects of Incidence

3.2.1 Low canard configuration

The effects of incidence on the vortex flow over the canard configurations are discussed using the examples described in Section 3.1. Figs.7 and 8 show, respectively, plan views and side views of a typical low canard configuration at angles of incidence of 12° , 15° , and 18° .

At an incidence of 12° , each canard vortex passes downstream over the canard trailing edge and appears to strike, or to pass very close to, the wing leading edge. At the point where the canard

vortex core strikes the leading edge, the wing vortex starts. This point is at about the 25% wing chord station. There is no discernible separate canard vortex above the wing, and in fact, the wing vortex looks like a continuation of the canard vortex. There is no vortex bursting over the wing.

At an incidence of 15° , each canard vortex passes just above the wing leading edge. The wing vortex originates from a point on the wing leading edge close to where the canard vortex passes over it, at about the 20% chord station. The canard vortex can be distinguished for a short distance downstream of the leading edge, as it interacts with the wing vortex. The canard and wing vortex cores merge into a single core beyond the 40% chord station, and each of the merged vortices bursts in the vicinity of the trailing edge.

At an incidence of 18° , each canard vortex passes higher over the wing leading edge than was the case at 15° . The wing vortex starts from the leading edge at about the 15% chord station. The canard and wing vortices intertwine, with the canard vortex remaining discernible for several turns. The canard vortex first passes directly beneath the canard vortex at about 45% chord. The two vortices have merged by about the 75% chord station. The merged vortex appears to burst at, or just downstream of, the trailing edge.

Figs.9 and 10 show, respectively, plan views and side views of the low canard configuration at angles of incidence of 20° , 25° , and 30° . The trends noted at lower angles of incidence continue. The canard vortices pass higher over the wing leading edges as incidence increases, and the intertwining of the canard and wing vortices occurs further downstream.

Fig.11 shows how the canard vortex position over the wing at the 25% chord station varies with incidence. (Results for $l/c = -0.2$ and 0.0 are also included.) The canard vortex generally moves upward and inward as incidence increases.

At an incidence of 20° , the wing vortices start from the leading edge at about the 15% chord station. The initial separation between the canard and wing vortices is greater than at lower angles of incidence, and the intertwining of the vortices occurs further downstream. The canard vortex first passes directly beneath the wing vortex at about 50% chord.

Fig.9 illustrates the way in which the canard vortex displaces the wing vortex outboard, just downstream of the point of origin of the latter. The wing vortex remains very close to the leading edge and begins to curve inboard only at about the 30-35% chord station.

Some asymmetry in the flow pattern is apparent. The left hand canard vortex crosses the wing leading edge slightly further upstream than does the right hand one. The left hand canard and wing vortices intertwine but both of them burst before merging is complete. The right hand canard and wing vortices intertwine and merge completely without any sign of vortex bursting over the wing in either the individual vortices or the merged vortex.

At an incidence of 25° , the wing vortex originates at about the 10% wing chord station, and again lies very close to the wing leading edge, back to 30-35% chord. The intertwining of the vortices occurs still further downstream than is the case for 20° incidence, with the canard vortex first passing under the wing vortex at about 60% chord. In this case, the flow pattern is more symmetrical, and before merging of the vortices is complete, all four cores have burst at 70-75% chord.

At an incidence of 30° , the wing vortices originate just upstream of the 10% chord station and, as for the lower incidences, remain close to the leading edge back to the 30% chord station. The canard and wing vortices all burst at 50-60% chord, before the canard vortices have started to move outboard beneath the wing vortices.

3.2.2 High canard configuration

Figs.12 and 13 show, respectively, plan views and side views of a typical high canard configuration ($h/c = 0.1$, $l/c = -0.1$) at angles of incidence of 12° , 15° , and 18° .

At an incidence of 12° , each canard vortex passes downstream well above the wing, moving inboard slightly under the influence of the wing vortex flowfield. The wing vortex originates at the wing apex. Seen in side view, as each canard vortex passes over the canard trailing edge, it begins to curve upwards to align itself with the freestream flow. As it comes under the influence of the wing vortex, the canard vortex curves downward again, towards the wing. The separation between the canard and wing vortices remains sufficiently great that at no stage do the vortices intertwine or merge over the wing.

At an incidence of 15° , the general features of the vortex flow pattern are similar to those at 12° . The downwards curvature of canard vortices over the wing is slightly more pronounced. Again, there is no intertwining or merging of the canard and wing vortices.

At an incidence of 18° , the flow pattern is generally similar to those at 12° and 15° .

Figs.14 and 15 show, respectively, plan views and side views of the high canard configuration at angles of incidence of 20° , 25° , and 30° .

At an incidence of 20° , the vortex pattern remains generally similar to that at lower angles of incidence. However, in this case, the wing vortices burst close to the wing trailing edge. The canard vortices remain unburst, although there is some thickening of their cores in the vicinity of the wing trailing edge.

At an incidence of 25° , the vortex pattern remains unchanged in its general features. However, the position of the burst in the wing vortex has moved upstream to about 70% of the wing chord. There appears to be some thickening of the canard vortex cores in the same region, indicating some form of breakdown in these vortices also.

At an incidence of 30° , the general flow pattern is similar to those described above, but the wing vortices burst at about 30% of the wing chord, and the canard vortices burst in about the same position. Downstream of the canard vortex burst, the turbulent canard vortex core is still deflected downwards under the influence of the flowfield of the burst wing vortices.

Er-EI and Seginer¹¹ describe generally similar flow patterns obtained using schlieren techniques in a wind tunnel. Their model had a high-canard configuration, with a wing sweep of 60° and a canard sweep of 75° . The downward movement of the canard vortices over the wing was more pronounced than in the present tests. This may be due, at least in part, to the smaller vertical separation ($h/c=0.08$) of the wing and canard on the wind-tunnel model, and to the higher sweep of the canard leading-edge.

3.2.3 Mid-canard configuration

The term "mid-canard" is used to describe a configuration with $h/c = 0.0$, in which the wing and the canard lie in the same plane. Figs.16 and 17 show, respectively, plan views and side views of the flow round a typical mid-canard configuration ($l/c = -0.1$) at angles of incidence of 12° , 15° , and 18° . As might be expected, the mid-canard flow patterns contain features of both the high canard and low canard patterns, depending on the angle of incidence under consideration.

At an angle of incidence of 12° , the canard vortex passes above the wing leading edge and curves downward under the influence of the wing vortex. The wing vortex originates from a point on the leading edge at about the 25% chord station. There is no intertwining or merging of the vortices.

At 15° incidence, the flow pattern is similar, except that the downward deflection of the canard vortex over the wing is greater.

At 18° incidence, the canard vortices, after being deflected inboard slightly by the wing vortices, move outboard slightly again. Thickening of the canard vortex cores in the vicinity of the wing trailing edge indicate the possible occurrence of vortex bursting there.

Plan views and side views of the mid-canard configuration are shown in Figs.18 and 19 for angles of incidence of 20° , 25° , and 30° . The trends apparent at the lower incidences are continued to these higher values. At an incidence of 20° , the wing vortices burst at about 85% of the wing chord. At an incidence of 25° , the wing vortex burst position has moved upstream to about 50% chord, and at an incidence of 30° , to about 40% chord.

3.3 Effect of Canard Longitudinal Position

3.3.1 Low canard configuration

Figs.20 and 21 show, respectively, plan views and side views of typical vortex patterns over a low canard configuration ($h/c = -0.1$) as the longitudinal position of the canard is varied from $l/c = -0.2$ to $l/c = 0.2$. The angle of incidence is 18° .

With the canard at the most upstream position ($l/c = -0.2$) each canard vortex passes well above the wing leading edge at about 20% chord, then curves downwards and outboard beneath the wing vortex. The wing vortex originates at about 15% chord, inboard of the canard vortex position at that station. The canard vortex core first passes directly beneath the wing vortex core at about the 60% chord station. The canard and wing vortices subsequently intertwine and merge near the wing trailing edge. There is no bursting in any of the vortices.

With the canard at the $l/c = -0.1$ position, the flow pattern is generally similar to that described above for $l/c = -0.2$, except that each canard vortex passes closer to the wing leading edge and the canard vortex core first passes directly underneath the wing vortex core at about the 45% wing chord station.

With the canard at the $l/c = 0.0$ position, the canard vortex crosses the wing leading edge at about 20% chord, and the wing vortex originates at the same station. The canard vortex merges almost immediately with the wing vortex, and the merged vortex bursts over the wing, in the 60-75% chord region.

Fig.11 shows how the canard vortex position over the wing at the 25% chord station moves downward and outboard as canard is moved aft.

With the canard at the $l/c = 0.1$ position, the vortex pattern changes from that observed for the more upstream canard positions. Under the influence of the wing flowfield, each canard vortex bursts in the vicinity of the canard trailing edge, and the expanded canard vortex core downstream of the burst strikes the wing leading edge. The wing vortex originates in the vicinity of this point, but this vortex itself bursts almost as soon as it has formed.

With the canard at the $l/c = 0.2$ position, each canard vortex bursts at about the 80% canard chord position. The turbulent flow downstream of the burst strikes the wing leading edge and causes disordered flow over the wing, with no evidence of the formation of a wing vortex.

The behaviour of the canard and wing vortices as the canard trailing edge position is moved downstream past the wing apex is very sensitive to the actual canard position. As the value of l/c is increased positively from zero, the position of the burst in the core of the merged canard and wing vortices moves rapidly upstream towards the wing leading edge. A situation is reached where each canard vortex remains unburst up to the wing leading edge, but the wing vortex bursts just behind the leading edge. This is shown in the photograph in Fig.22, with the canard position at $l/c = 0.08$. The canard vortex core appears to be unburst, right up to the point where it strikes the wing leading edge. The wing vortex, on the other hand, bursts almost as soon as it has formed.

To examine in some more detail the type of flow pattern in which the canard vortex core passes very close to, or strikes, the wing leading edge, a configuration with $l/c = 0.05$ was tested. Use was made of the flexibility of the hydrogen bubble system, which allows the electrodes on the canard and wing leading edges to be energised independently. Fig.23 shows plan views of the configuration with only the wing cathodes energised (Fig.23(a)), only the canard cathodes energised (Fig.23(b)), and

with all cathodes energised (Fig.23(c)). Fig.24(a)-(c) shows side views with the same cathode arrangements. The angle of incidence is 18° .

Figs.23(a) and 24(a), with bubbles from only the wing leading edges, show that the point of origin of the wing vortex is at about the 25% chord station on the wing leading edge. The wing vortex bursts at about 45% chord. Figs.23(b) and 24(b), with bubbles from only the canard leading edges, show that the canard vortex core passes very close to the wing leading edge, and that the hydrogen bubbles in the canard vortex core are carried directly into the wing vortex core. Figs.23(c) and 24(c), with bubbles from both canard and wing leading edges, confirm that the canard and wing vortices have merged over the wing.

It is apparent from Figs.23 and 24 that in cases like this where the canard vortex core passes very close to or strikes the wing leading edge, the cores of the canard and wing vortices become essentially continuous. The scale of the model and the resolution of the flow visualisation system did not permit a detailed study of the vortex core structure in the region of the leading edge, but it appears that the merging of the canard and wing vortex cores takes place within a very short distance of the point of origin of the wing vortex.

3.3.2 High canard configuration

Figs.25 and 26 show, respectively, plan views and side views of typical vortex patterns over a high canard configuration ($h/c = 0.1$) as the longitudinal position of the canard is varied from $l/c = -0.2$ to $l/c = 0.2$. The incidence is 18° .

For the high canard configuration, the effects of changes in canard longitudinal position on the vortex patterns are less apparent than is the case for the low canard configuration. For the $l/c = -0.2$ position, each canard vortex passes downstream past the canard trailing edge and is deflected downwards and slightly inboard as it comes under the influence of the wing vortex flowfield. The wing vortex originates at the wing apex. The spacing between the canard and wing remains sufficiently great that intertwining and merging of the vortex cores do not occur.

As the canard surface is shifted aft relative to the wing, the general features of the flow pattern remain similar. The vertical separation between the canard and wing vortices decreases, but the horizontal separation changes little, and at no stage do the canard and wing vortices intertwine or merge. The wing vortices originate at the wing apex for all the canard positions. The influence of the canard vortex flowfield is insufficient to displace the wing vortex origin outboard along the leading edge.

The interaction between the canard and wing flowfields has a beneficial effect on vortex breakdown when compared to the situation for the low canard. As the high canard is moved aft, the wing vortices remain unburst over the wing, and bursts appear in the canard vortices only for the rearmost canard position tested. Even in this case, the canard vortices do not burst until a station in the vicinity of the wing trailing edge is reached.

3.3.3 Mid-canard configuration

Figs.27 and 28 show, respectively, plan views and side views of typical vortex patterns over a mid-canard or co-planar configuration ($h/c = 0.0$) as the longitudinal position of the canard is varied from $l/c = -0.2$ to $l/c = 0.0$. The incidence again is 18° . The flow patterns show greater similarity to those for high-canard configurations than to those for low-canard configurations.

For the most forward canard position, the canard vortex is deflected downwards over the wing, under the influence of the wing vortex flowfield. The canard vortex core first reaches the same horizontal level as the wing vortex core at a station slightly downstream of the wing trailing edge. The canard vortex core is deflected inboard slightly over the wing, and begins to curve outboard slightly in the vicinity of the wing trailing edge. The wing vortex origin is displaced outboard along the leading

edge, to about the 15% chord station. The canard vortices burst at about 80-85% wing chord. The left-hand wing vortex bursts just downstream of the wing trailing edge.

As the canard is moved downstream, the flow pattern remains similar, except that the station at which the vortex core vertical crossover occurs moves upstream, to about 85% of the wing chord for $l/c = 0.0$. For this canard position also, the point of origin of the wing vortex has moved downstream slightly, to about the 20% chord station. The pattern of vortex bursts remains unchanged except that there is now no sign of bursting in the wing vortices.

3.4 Effect of Canard Vertical Position

In Figs.29 and 30, the vortex patterns for three different canard vertical positions ($h/c = -0.1, 0.0, \text{ and } 0.1$) are compared, for $l/c = -0.1$ and an angle of incidence of 20° . The most obvious changes in the flow patterns occur between the low- and mid-canard configurations, as the degree of interaction between the wing and canard vortices decreases markedly. The displacement of the wing vortex origin away from the wing apex also decreases as the canard is raised relative to the wing.

3.5 Flow near Wing Apex

As has been noted above, there are some conditions, particularly with low-canard configurations, under which one effect of the canard is to displace the origin of the wing vortex from the wing apex to a point outboard along the wing leading edge. It is of interest to examine the behaviour of the flow in the vicinity of the wing leading edge in the region between the apex and the point of origin of the wing vortex. For most configurations, no clear structure could be discerned in this region. However, for a low canard configuration with the canard trailing edge at a distance of 5% of the wing chord behind the wing apex, some flow features were observed and were examined in more detail.

Fig.31(a) and (b) shows plan and side views of the flow pattern round this configuration at an incidence of 30° . Only the wing cathodes were energised for these photos. There appears to be a flow structure originating from a point on the wing lower surface, upstream of the wing vortex origin. This structure looks like a vortex core which curls up and around the leading edge and becomes entrained in the wing vortex system. Similar flow patterns were observed at 25° incidence.

It was difficult to illuminate satisfactorily the region of the flow beneath the wing apex, but by careful adjustment of a light on one side of the towing carriage and a camera on the opposite side, it was possible to obtain some side view photographs, examples of which are shown in Fig.32(a) and (b). The angle of attack is 30° . The photographs were taken at Reynolds numbers of 5.2×10^4 and 9.8×10^4 respectively.

Each photograph shows what appears to be a vortex beneath the wing leading edge, with its core originating at or close to the wing apex. This part of the leading edge is immersed in the strong downwash and sidewash field inboard of and beneath the canard vortex. This velocity field maintains attached, outboard-moving flow over the wing upper surface. Separation occurs at the leading edge and the separated flow rolls up to form a small vortex beneath the leading edge.

In the vicinity of the point where the canard vortex core passes close to the wing leading edge, the local flowfield near the leading edge changes from a downwash to an upwash. The flow separating at the leading edge now forms the familiar vortex system above the wing. The underside vortex curves sharply upwards, passes round the leading edge, and merges into the interacting vortex systems above the wing. Another photograph of the flow pattern is presented in Fig.33, which shows a perspective view from a point above and behind the model, at a Reynolds number of 5.3×10^4 . The underside vortex can be seen looping around the leading edge, outboard of the point where the wing upper surface vortex core originates.

Fig.34 shows the relative positions of the undersurface vortex, the wing vortex, and the canard vortex at an incidence of 30° , and a Reynolds number of 5.3×10^4 . Both canard and wing electrodes were energised, and the photo was taken from a video display.

3.6 Effect of Canard on Vortex Breakdown

It is apparent from the flow patterns described so far that the relative positions of the wing and canard have a marked effect on the occurrence of breakdown within the wing and canard vortices. In Fig.35, measured positions of wing vortex breakdown are plotted against incidence for several values of longitudinal canard position, for each of the three vertical canard positions tested. Also included are lines showing vortex breakdown positions for the wing alone case.

For the high- and mid-canards, breakdown occurs further downstream than is the case for the wing alone. The shift is quite substantial. For example, at an incidence of 20° , the breakdown typically moves downstream from about the 40% wing chord station to the trailing edge. The actual longitudinal position of the canard has a lesser effect. The most forward position ($l/c = -0.2$) causes the smallest breakdown shift, but the difference in shift magnitude between the most forward and most aft canard positions is only some 20% of the wing chord. Er-EI and Seginer¹¹ and Werlé¹³ found similar favourable canard effects on wing vortex breakdown position in their tests of high and mid-canard configurations.

The longitudinal position of the low canard is much more critical. The most forward position produces a breakdown shift of about the same magnitude as the high and mid-canards. However, as the low canard is moved aft, the breakdown shift is considerably reduced, particularly at the lower angles of incidence. In fact, a low canard can reverse the breakdown shift, causing the wing vortex to burst further upstream than it would over the wing alone. The incidence at which the reversal occurs increases as the canard is moved aft. As discussed above, when the canard trailing-edge is moved aft past the wing apex, the interaction of the canard vortex and the wing leading-edge causes the wing vortex to burst almost as soon as it forms. Thus the most upstream vortex breakdown positions plotted in Fig.35 for the low canard at $l/c > 0$ correspond closely to the points of origin of the wing vortices.

The interaction of the wing and canard in general has a favourable effect on vortex breakdown over the canard itself. For an isolated delta wing, vortex breakdown moves upstream with increasing incidence, crossing the trailing-edge at an incidence of about 30° . For almost all of the configurations tested, except for the aft positions of the low canard, the canard vortices burst well downstream of the canard trailing-edge. This favourable effect was noted by Behrbohm⁷, and by Hummel and Oelker¹⁰.

An unusual effect was noted in the canard vortices over the mid-canard configuration, with the canard in its most forward position ($h/c=0$, $l/c=-0.2$), at an incidence of 30° . This was the apparent re-formation of the canard vortex cores downstream of breakdown points. A plan view of the flow pattern is shown in Fig.36(a), at a Reynolds number of 9.5×10^4 . The right-hand canard vortex appears to have burst in the vicinity of the canard trailing edge. There is a region of turbulent flow downstream of the burst, but at a point about 10-15% of the wing chord behind the canard trailing edge, the canard vortex core appears to have formed again. The core passes downstream over the wing and bursts again at about the 50% wing chord station. A similar phenomenon was observed at an incidence of 25° , although the first burst of the canard vortex was less distinct than was the case at 30° .

An example of the flow pattern over the same configuration at a lower Reynolds number of 4.5×10^4 is shown in Fig.36(b). The angle of incidence is again 30° . In this case both canard vortices burst and reform. The initial burst occurs further upstream than was the case at the higher Reynolds number, and the streamwise distance between the initial burst and the reappearance of the core is greater.

The re-forming of the canard vortices is due presumably to favourable pressure gradients experienced by the vortices in the flow ahead of the wing. Hummel and Oelker¹⁰ observed a similar phenomenon in their water tunnel tests, and the restoration of a burst vortex in a tube by a favourable pressure gradient has been described by Harvey¹⁷.

4. CONCLUSIONS

The formation and interaction of vortices above a canard/wing configuration where canard and wing both had sharp, highly-swept leading edges were studied using flow visualisation techniques in a small towing tank. In general, the canard vortex system interacted with the wing vortex system to a degree dependent on the relative positions of the two surfaces.

The most extensive interaction occurred with the canard beneath the wing plane. In this case, the canard vortices intertwined and merged with the wing vortices, with the details of the interaction depending on the longitudinal position of the canard. Forward positions of the low canard delayed wing vortex breakdown, at least at higher angles of incidence. This favourable effect was reduced as the canard was shifted aft, and in its rearmost positions the low canard could seriously disrupt the wing vortex flow.

A canard above or co-planar with the wing produces less interaction between the vortex systems, and delays breakdown in the wing vortices.

Other features of the flow successfully visualised for some canard positions include vortex formation beneath the wing apex, and bursting and re-forming of the canard vortices.

REFERENCES

1. Burns, B.R.A. *Canards : design with care*
Flight International, 23 Feb., 19-21 (1985)
2. Nicholas, W.U.
Neville, G.L.
Hoffschwelle, J.E.
Huffman, J.K.
Covell, P.F. *An evaluation of the relative merits of wing-canard, wing-tail, and tailless arrangements for advanced fighter applications*
14 th. Congress of the Aeronautical Sciences, Proceedings, Paper ICAS-84-2.7.3 (1984)
3. Gloss, B.B.
McKinney, L.W. *Canard-wing lift interference related to maneuvering aircraft at subsonic speeds.*
NASA TM-X-2897 (1973)
4. Ottensoser, J. *Parametric analysis of close-coupled canard transonic aerodynamics for a generalized wing-body configuration.*
David Taylor NSRDC, Rept No. DTNSRDC/ASED-399
5. Hale, R.W.
Tan, P.
Ordway, D.E. *Prediction of aerodynamic loads on close-coupled canard configurations - Theory and experiment.*
Sage Action Inc., Rept. No. SAI-RR-7702 (1977)
6. Paulson, J.W.
Thomas, J.L. *Summary of low-speed longitudinal aerodynamics of two powered close-coupled wing-canard fighter configurations.*
NASA-TP-1535 (1979)
7. Behrbohm, H. *Basic low speed aerodynamics of the short-coupled canard configuration of small aspect ratio.*
SAAB-TN-60 (1965)

8. Karling, K. *Aerodynamics of the Viggen 37 aircraft. Part 1: General characteristics at low speed.*
NASA TM-88403 (1986)
(Transl. from SAAB book of same title, 1975)
9. Calarese, W. *Vortex interaction on a canard-wing configuration.*
AFWAL-TR-86-3100 (1986)
10. Hummel, D.
Oelker, H. *Vortex interference effects on close-coupled canard configurations in incompressible flow.*
Symp. on Intl. Vortex Flow Experiment on Euler Code Validation, Proceedings, Stockholm, 47-61 (1986)
11. Er-EI, J.
Seginer, A. *Vortex trajectories and breakdown on wing-canard configurations.*
AIAA J. of Aircraft, 22, 8, 641-648 (1985)
12. Er-EI, J. *Effect of wing/canard interference on the loading of a delta wing.*
AIAA J. of Aircraft, 25, 1, 18-24 (1988)
13. Werlé, H. *Vortex interactions on fixed and oscillating delta wings (water tunnel visualisations)*
La Recherche Aerospat., 1989/2, 43-68 (1989)
14. Schraub, F.A.
Kline, S.J.
Henry, J.
Runstadler, P.W.
Littell, A. *Use of hydrogen bubbles for quantitative determination of time-dependent velocity fields in low-speed water flows.*
ASME J. Basic Engineering, 87, 429-444 (1965)
15. Thompson, D.H. *Flow visualisation using the hydrogen bubble technique.*
ARL Aerodynamics Note 338 (1973)
16. Thompson, D.H. *A visualisation study of the vortex flow around double-delta wings.*
ARL Aerodynamics Report 165 (1985)
17. Harvey, J.K. *Some observations of the vortex breakdown phenomenon.*
J. Fluid Mech., 14, 585-592 (1962)

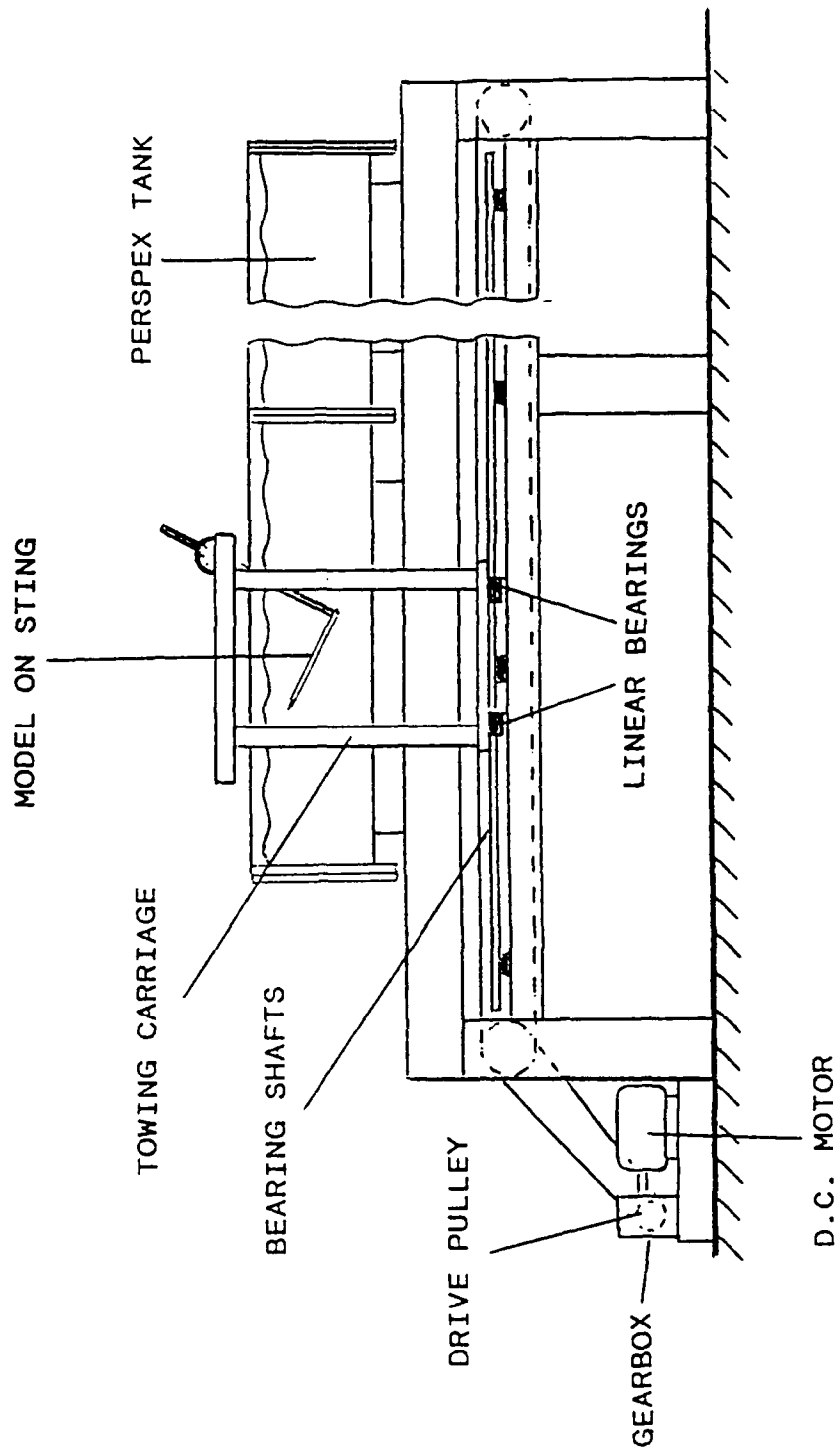


Fig.1 Towing tank used for flow visualisation tests

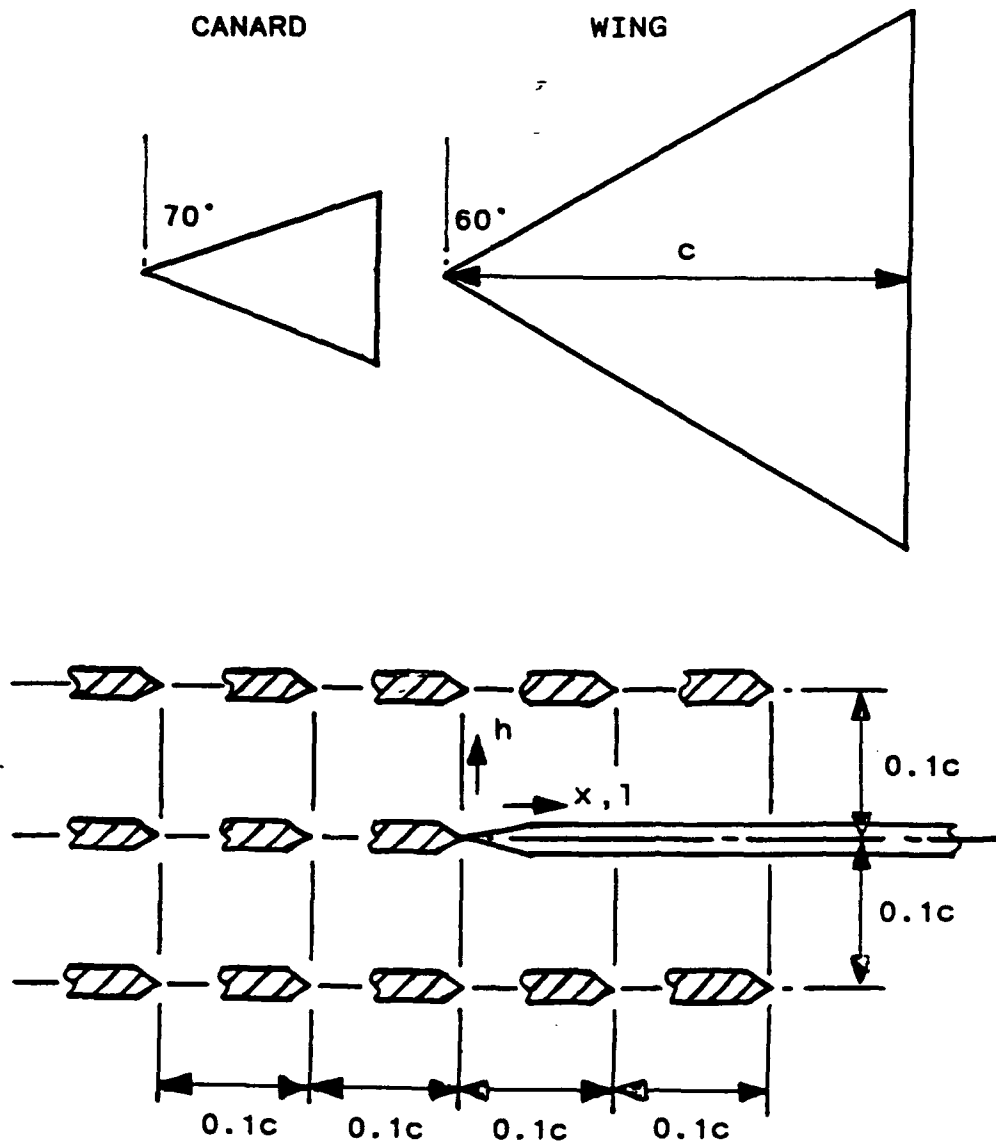


Fig.2 Range of canard / wing relative positions

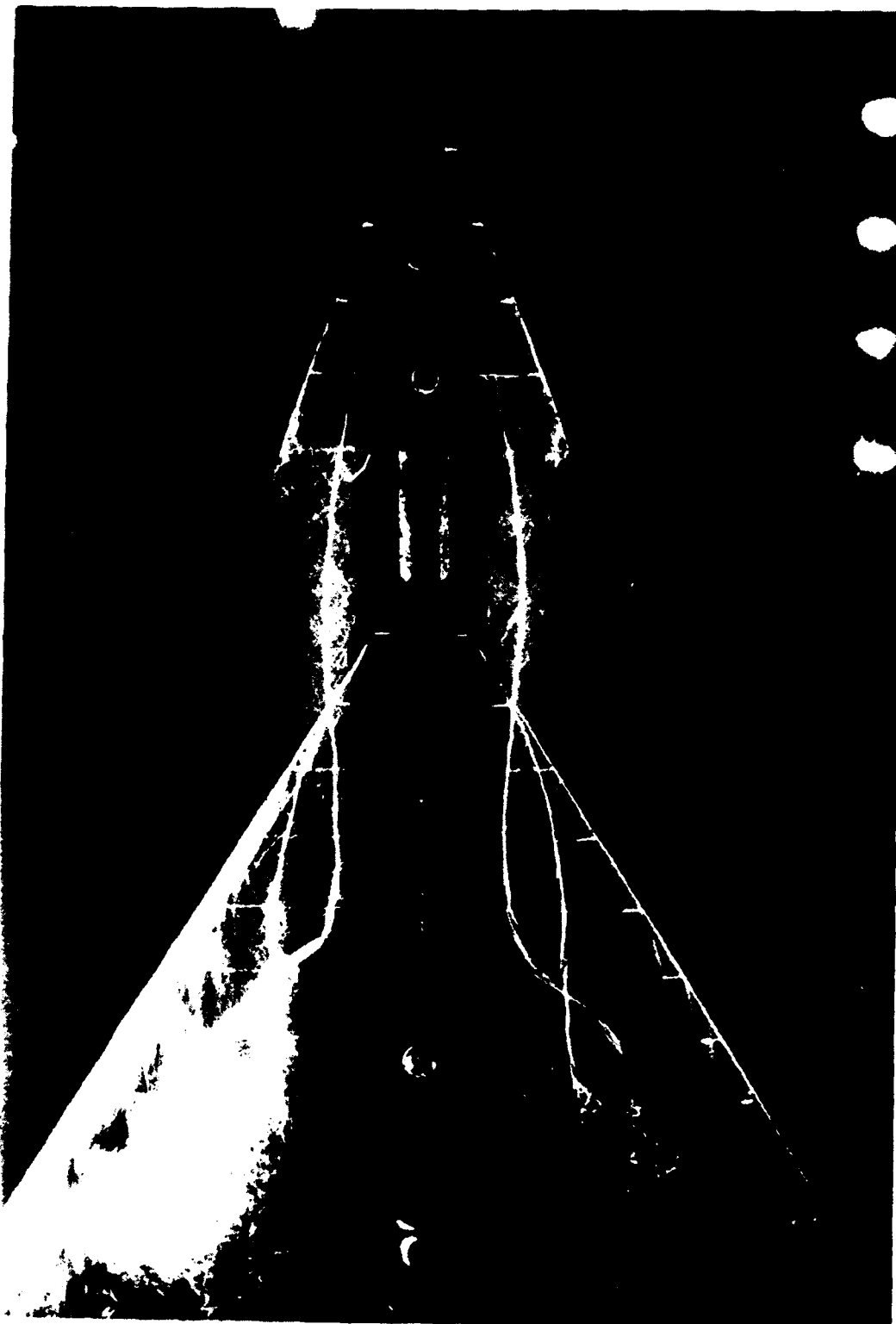


Fig.3 Vortex flow over typical low canard configuration
(Plan view)

(Angle of attack = 25° , $h/c = -0.1$, $l/c = -0.1$)

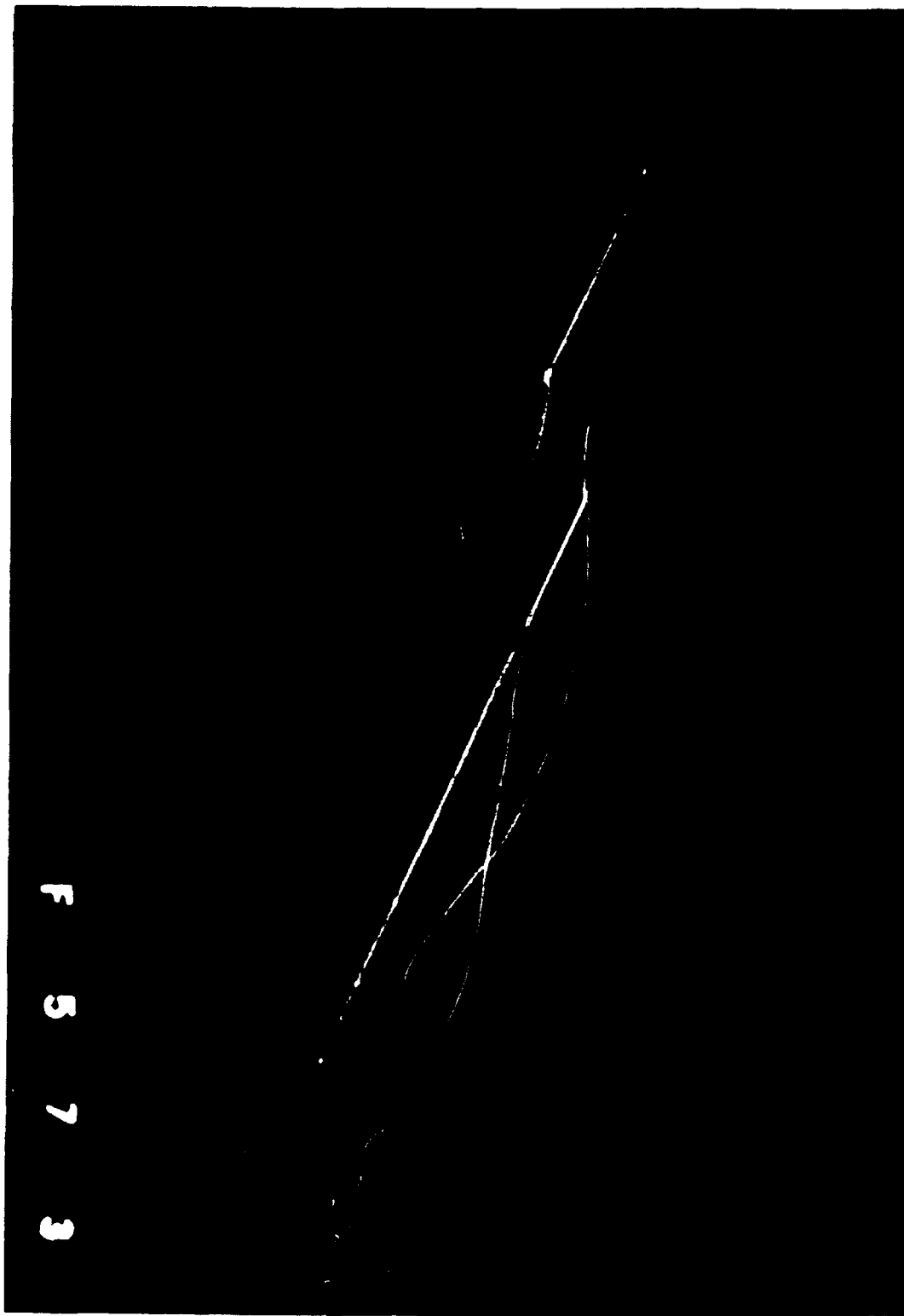


Fig.4 Vortex flow over typical low canard configuration
(Side view)

(Angle of attack = 25° , $h/c = -0.1$, $l/c = -0.1$)

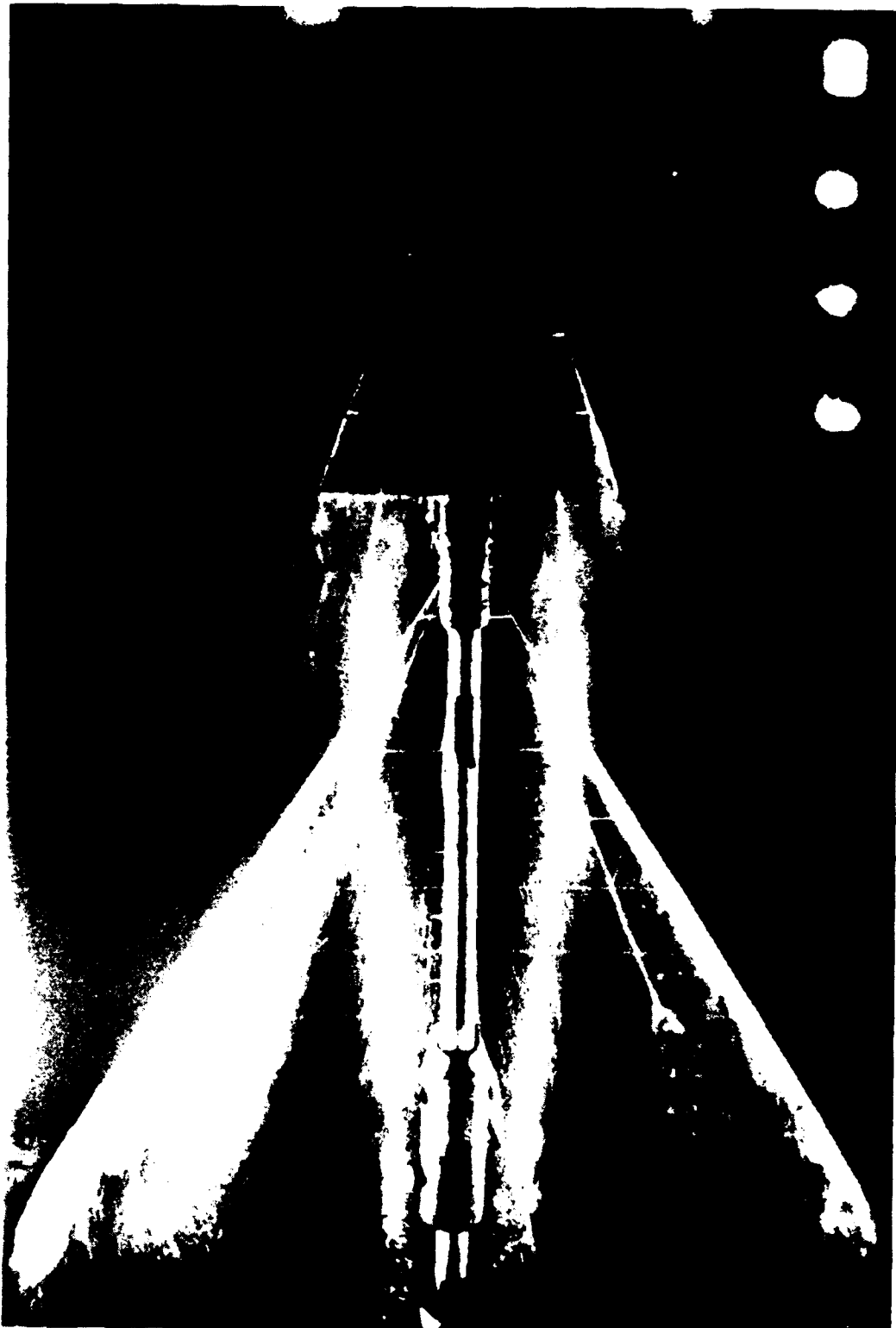


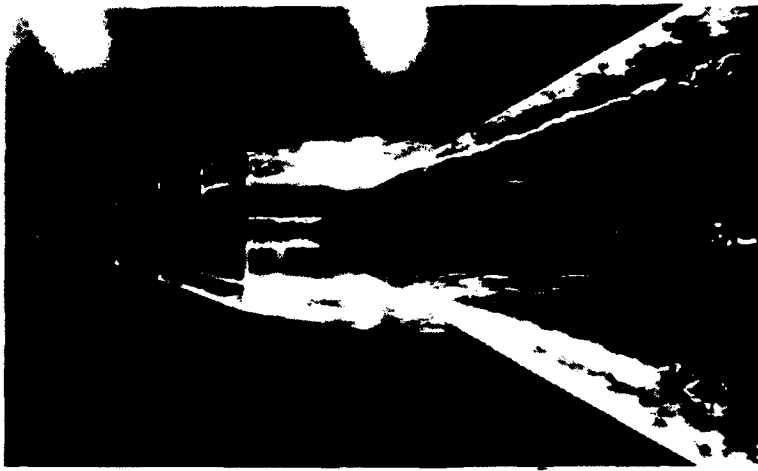
Fig.5 Vortex flow over typical high canard configuration
(Plan view)

(Angle of attack = 25° , $h/c = 0.1$, $1/c = -0.1$)

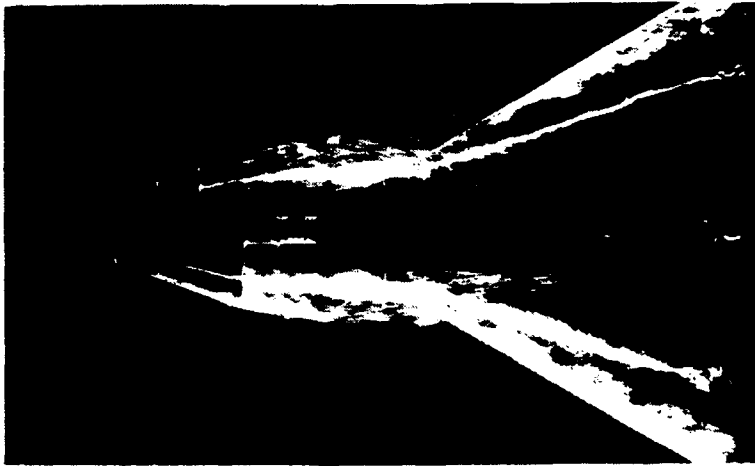


Fig.6 Vortex flow over typical high canard configuration
(Side view)

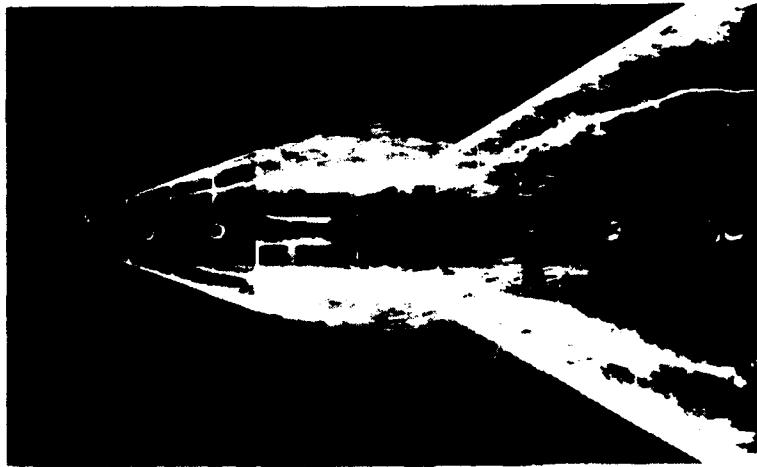
(Angle of attack = 25° $h/c = 0.1$, $l/c = -0.1$)



Angle of attack = 12°



Angle of attack = 15°

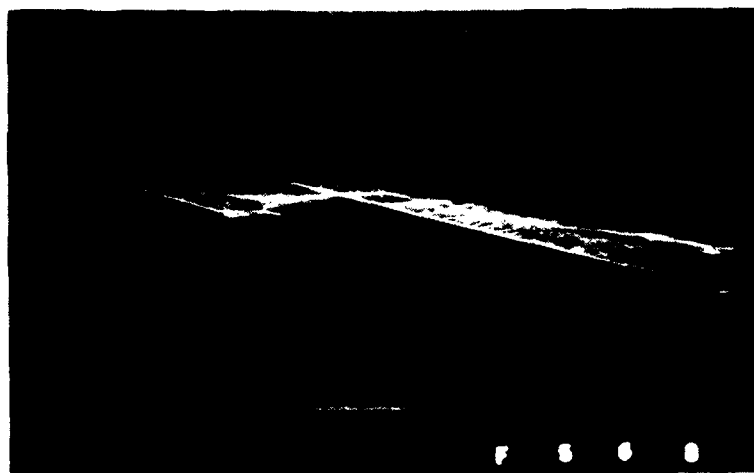


Angle of attack = 18°

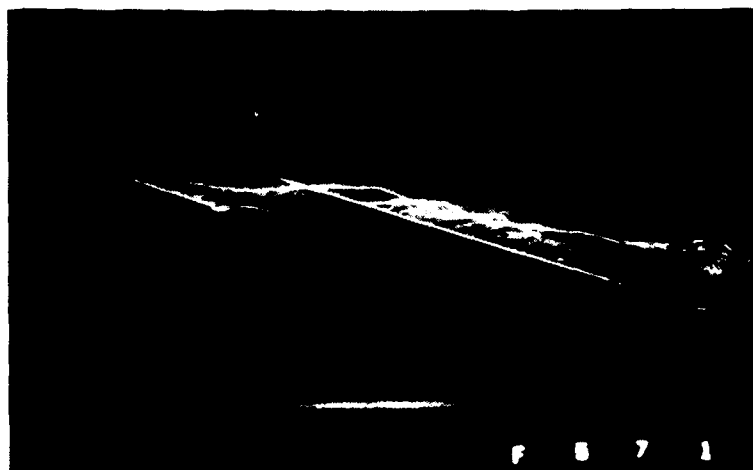
Fig.7 Effect of incidence on vortex flow over low canard configuration (Plan view)
($h/c = -0.1$, $l/c = -0.1$)



Angle of attack = 12°

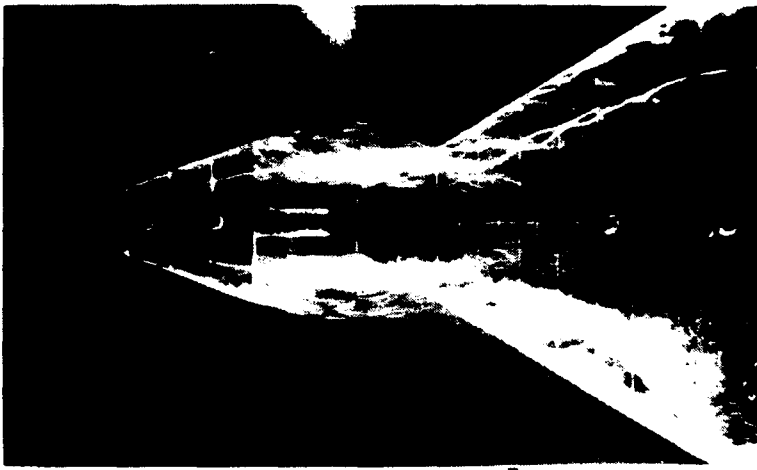


Angle of attack = 15°

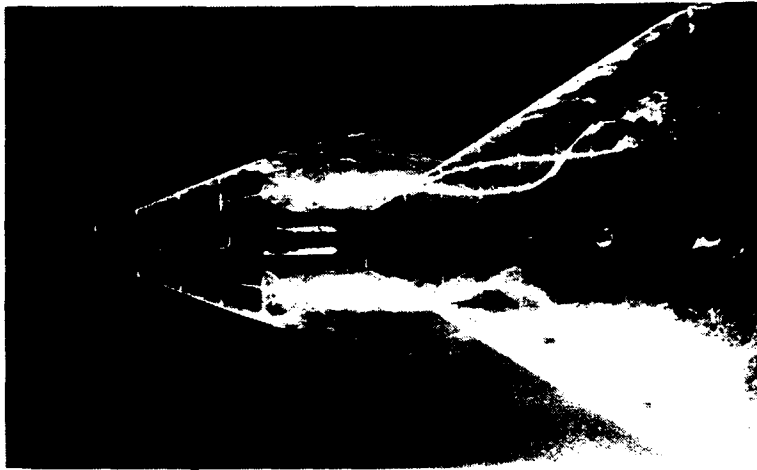


Angle of attack = 18°

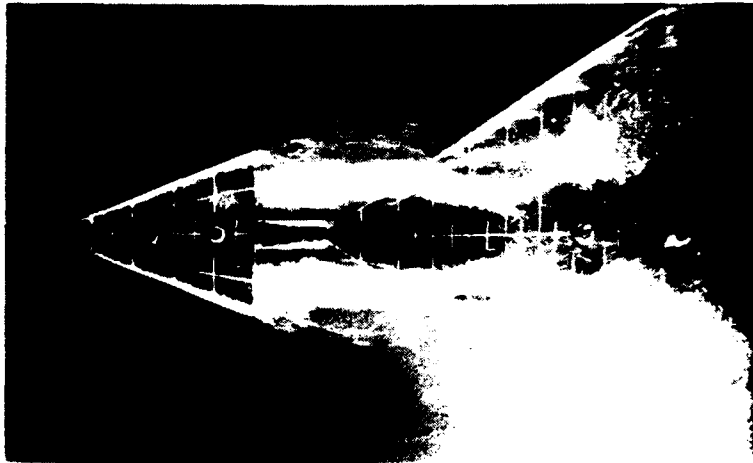
Fig.8 Effect of incidence on vortex flow over low canard configuration (Side view)
($h/c = -0.1$, $l/c = -0.1$)



Angle of attack = 20°



Angle of attack = 25°

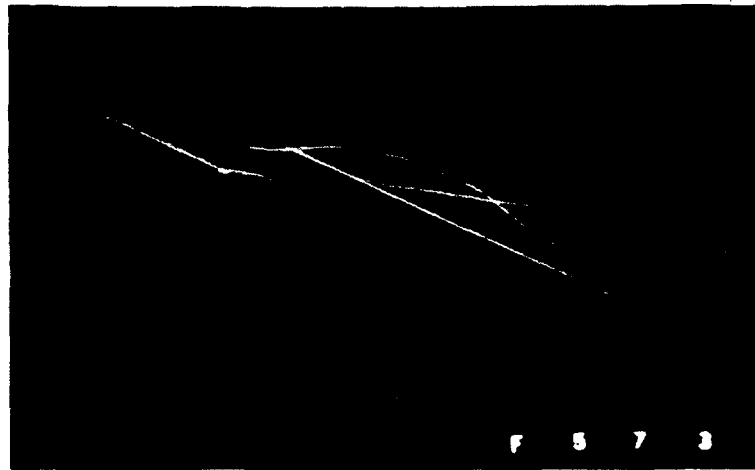


Angle of attack = 30°

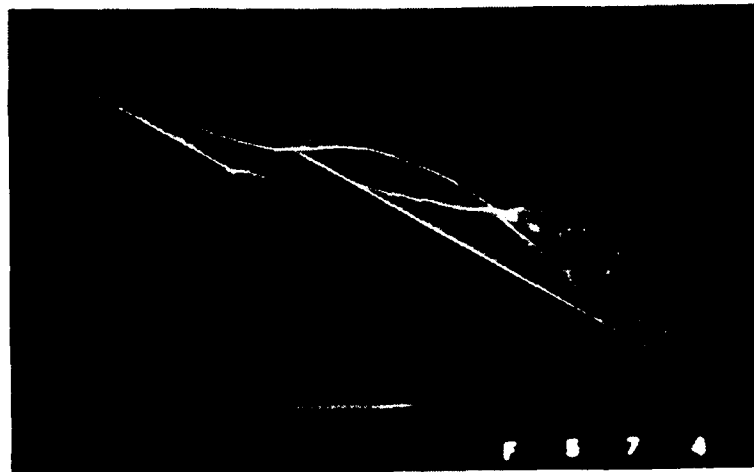
Fig.9 Effect of incidence on vortex flow over low canard configuration (Plan view)
($h/c = -0.1$, $l/c = -0.1$)



Angle of attack = 20°



Angle of attack = 25°



Angle of attack = 30°

Fig.10 Effect of incidence on vortex flow over low canard configuration (Side view)
($h/c = -0.1$, $l/c = -0.1$)

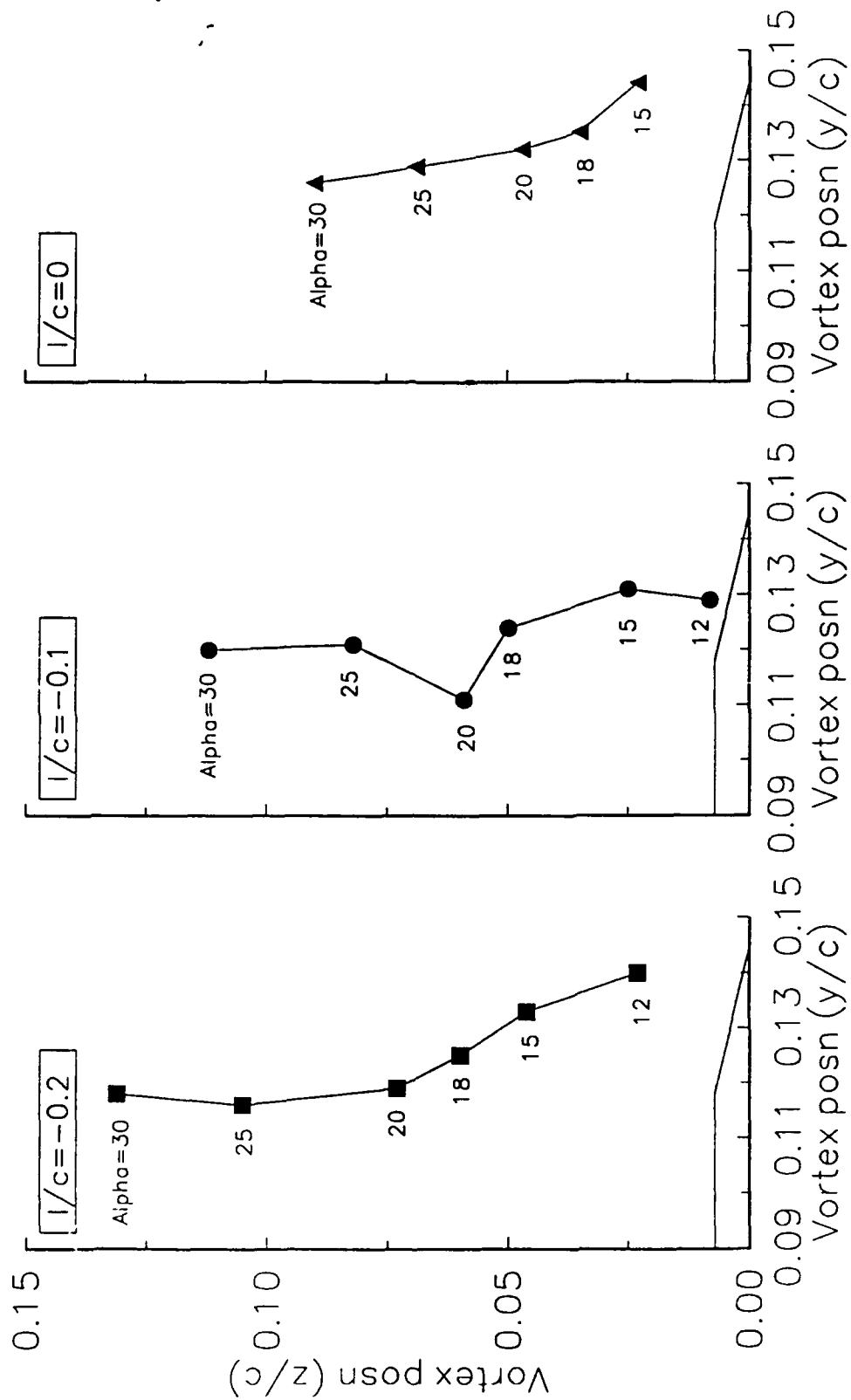
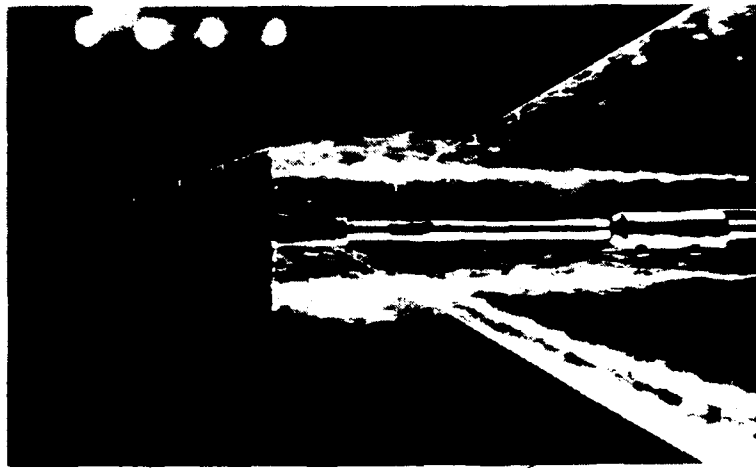
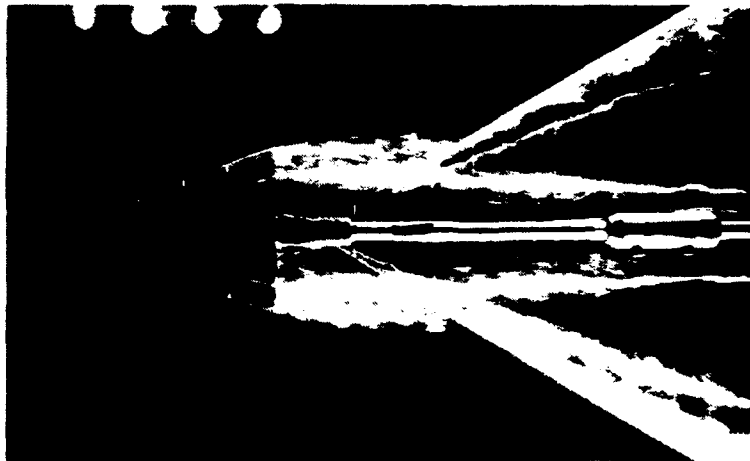


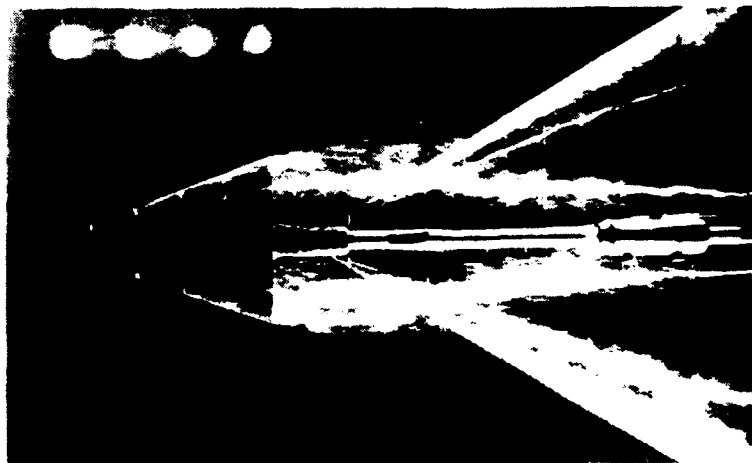
Fig.11 Effect of incidence on canard vortex position over wing at $x/c = 0.25$
($h.c = -0.1$)



Angle of attack = 12°



Angle of attack = 15°



Angle of attack = 18°

Fig.12 Effect of incidence on vortex flow over high canard configuration (Plan view)
($h/c = 0.1$, $l/c = -0.1$)



Angle of attack = 12°

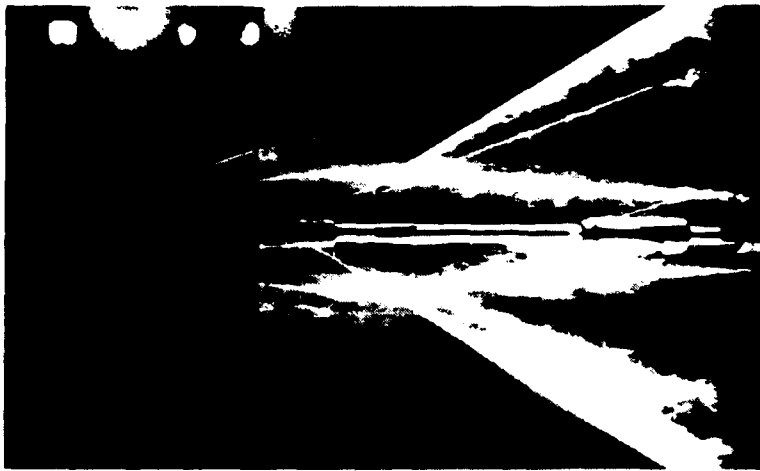


Angle of attack = 15°

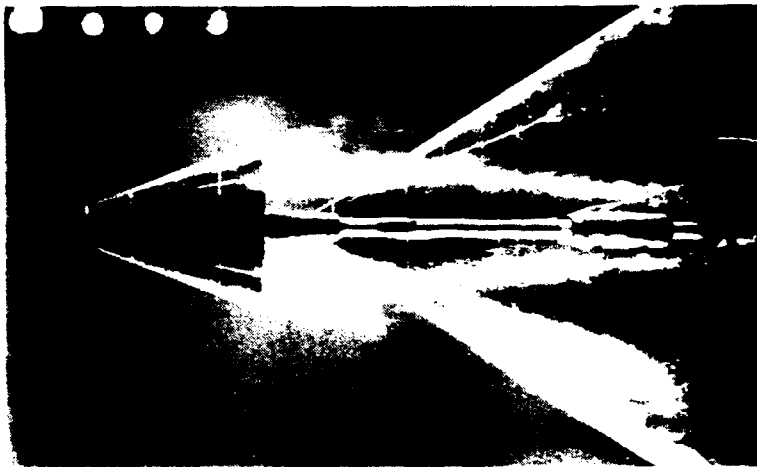


Angle of attack = 18°

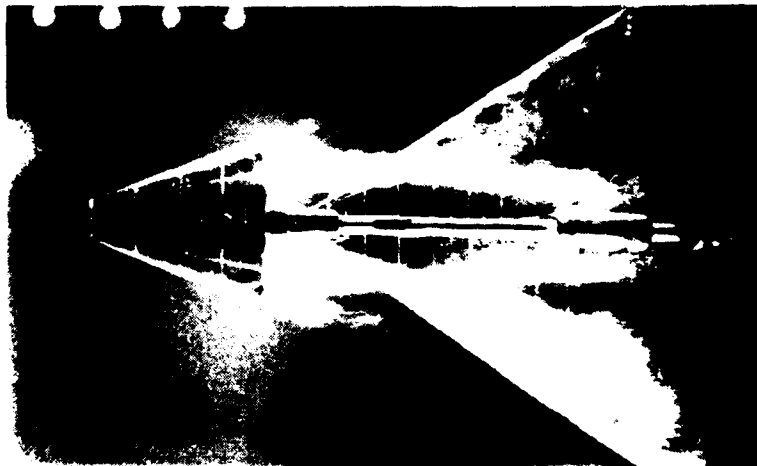
Fig.13 Effect of incidence on vortex flow over high canard configuration (Side view)
($h/c = 0.1$, $l/c = -0.1$)



Angle of attack = 20°

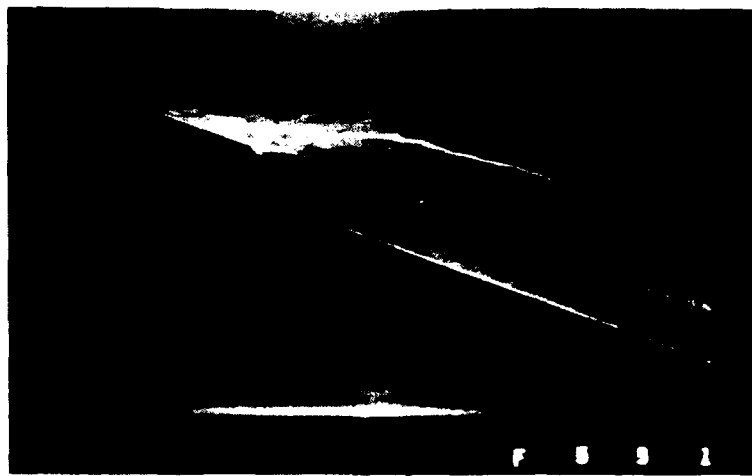


Angle of attack = 25°



Angle of attack = 30°

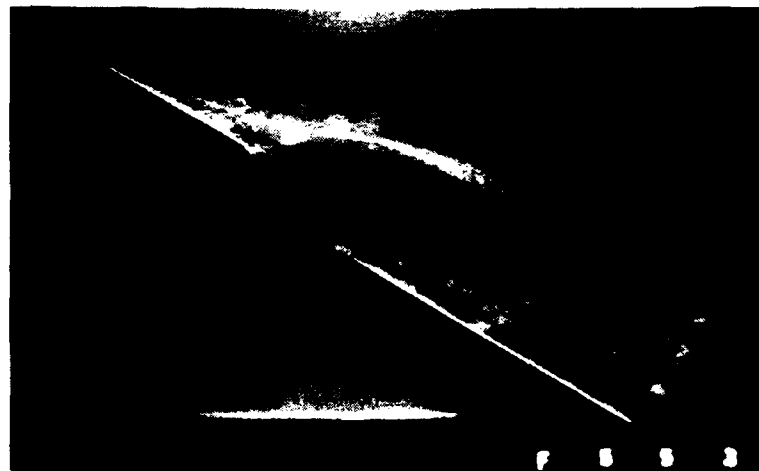
Fig.14 Effect of incidence on vortex flow over high canard configuration (Plan view)
($h/c = 0.1$, $l/c = -0.1$)



Angle of attack = 20°

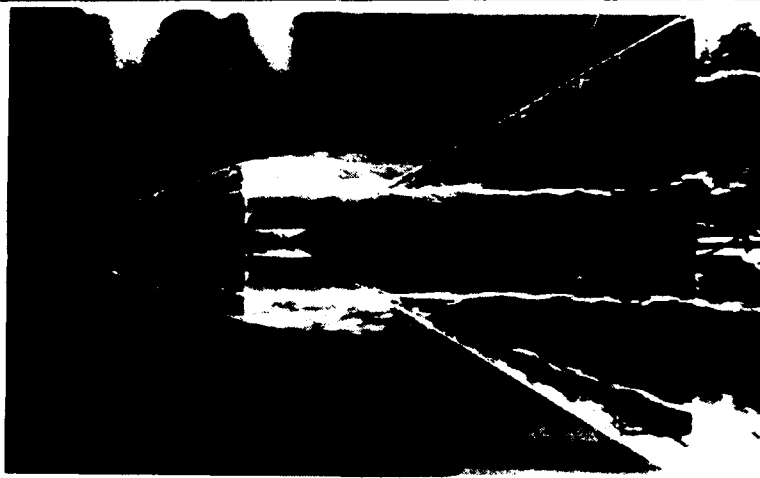


Angle of attack = 25°

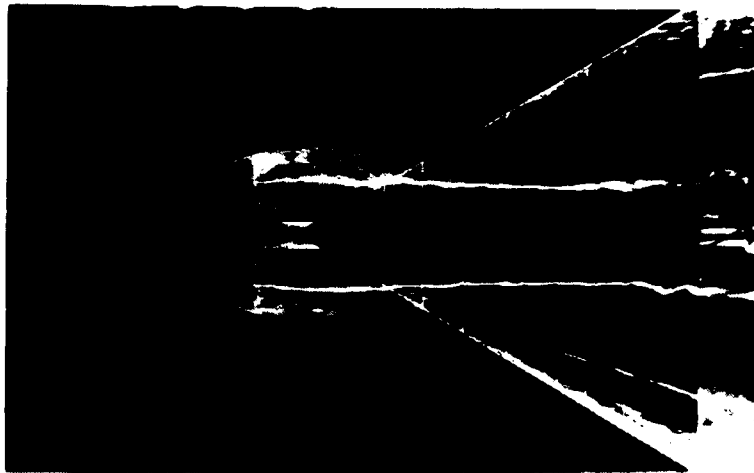


Angle of attack = 30°

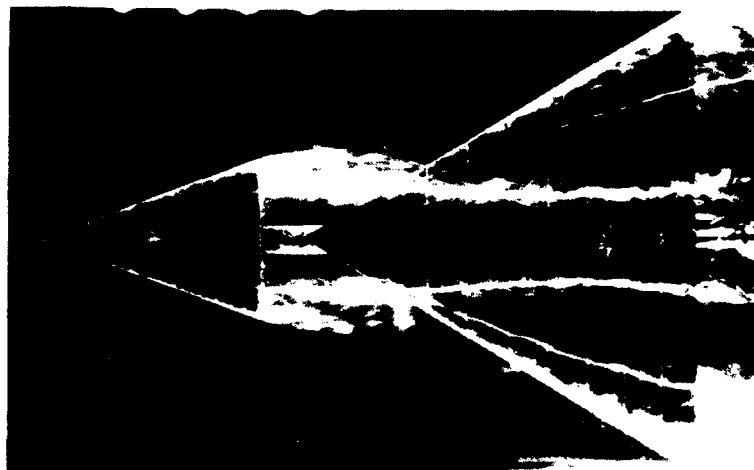
Fig.15 Effect of incidence on vortex flow over high canard configuration (Side view)
($h/c = 0.1$, $l/c = -0.1$)



Angle of attack = 12°

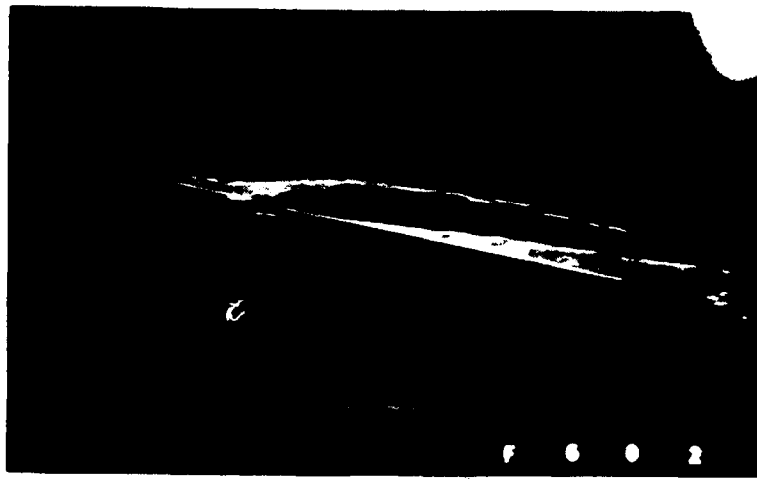


Angle of attack = 15°

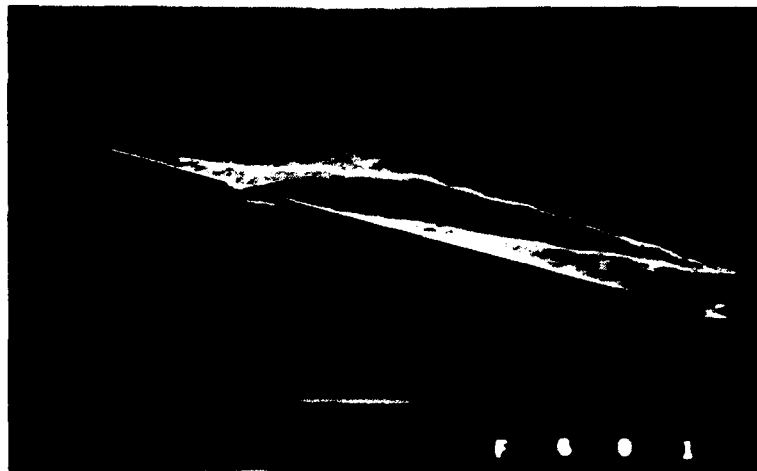


Angle of attack = 18°

Fig.16 Effect of incidence on vortex flow over mid-canard configuration (Plan view)
($h/c = 0$, $1/c = -0.1$)



Angle of attack = 12°

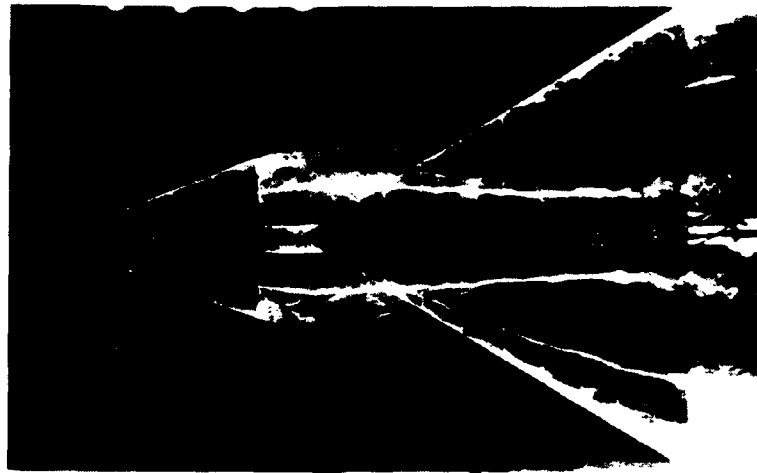


Angle of attack = 15°

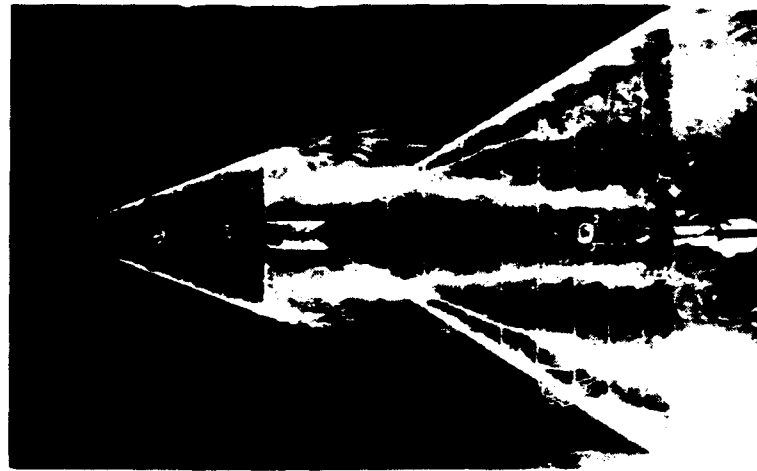


Angle of attack = 18°

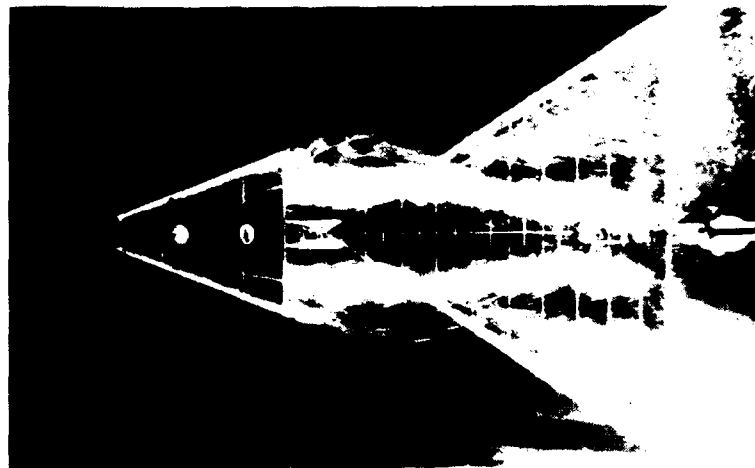
Fig.17 Effect of incidence on vortex flow over mid-canard configuration (Side view)
($h/c = 0$, $l/c = -0.1$)



Angle of attack = 20°

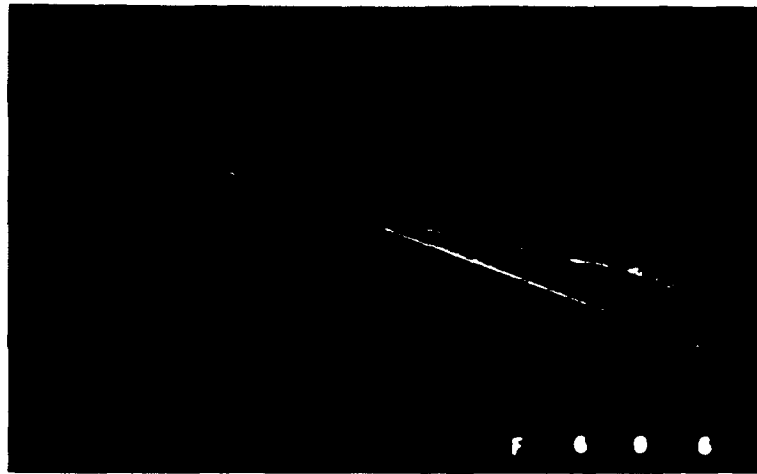


Angle of attack = 25°

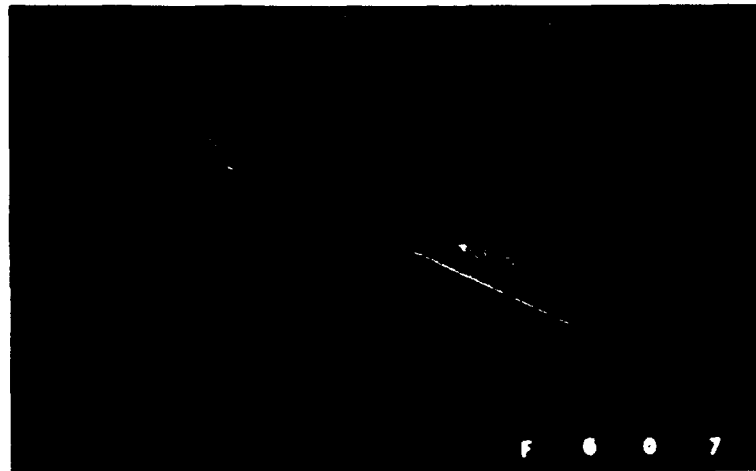


Angle of attack = 30°

Fig.18 Effect of incidence on vortex flow over mid-canard configuration (Plan view)
($h/c = 0$, $l/c = -0.1$)



Angle of attack = 20°

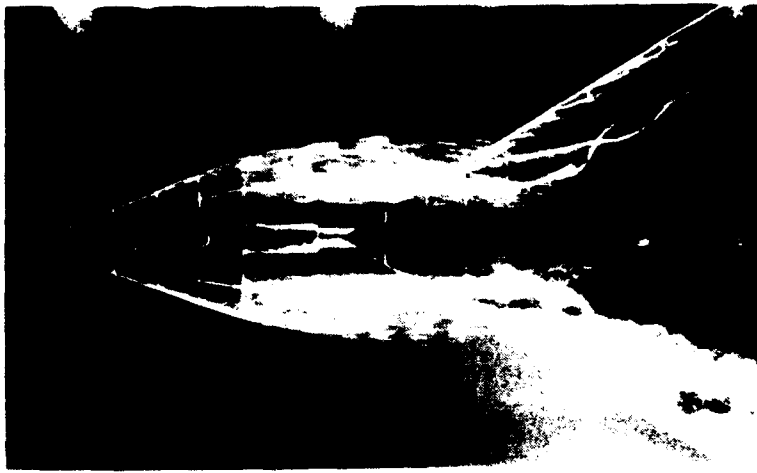


Angle of attack = 25°

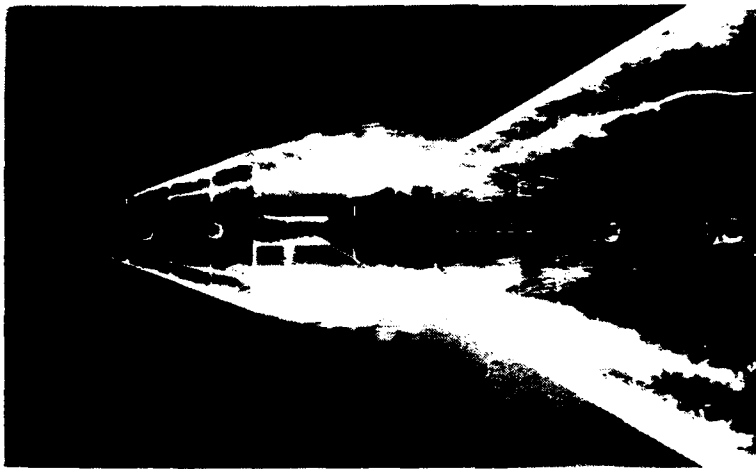


Angle of attack = 30°

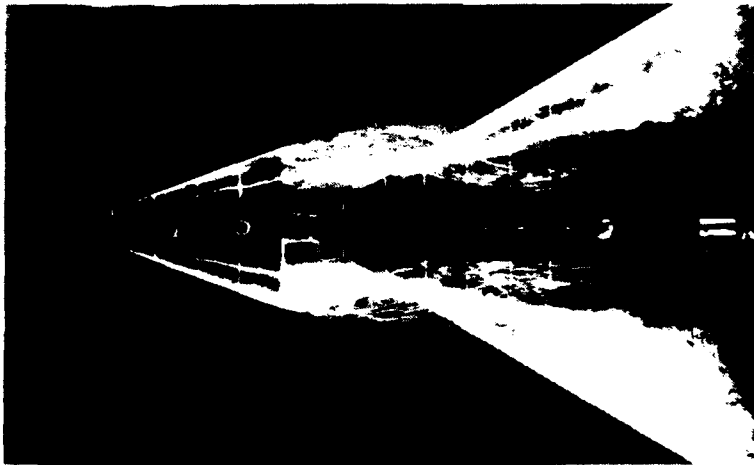
Fig.19 Effect of incidence on vortex flow over mid-canard configuration (Side view)
($h/c = 0$, $1/c = -0.1$)



$$1/c = -0.2$$

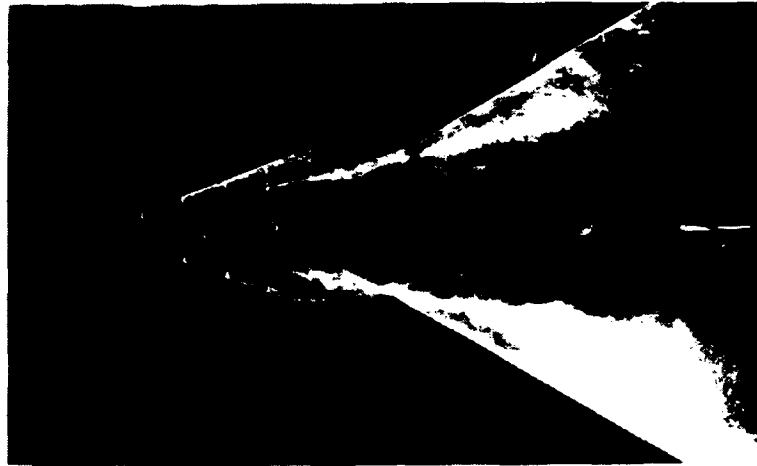


$$1/c = -0.1$$

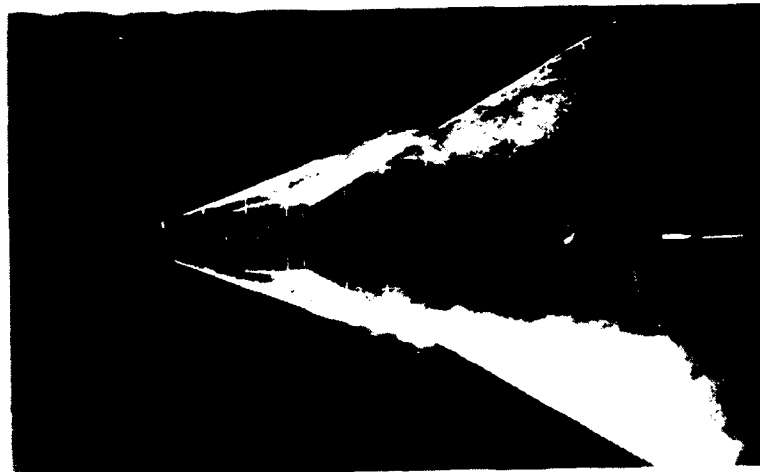


$$1/c = 0$$

Fig.20 Effect of canard longitudinal position on vortex flow over low canard configuration (Plan view)
(Angle of attack = 18° , $h/c = -0.1$)

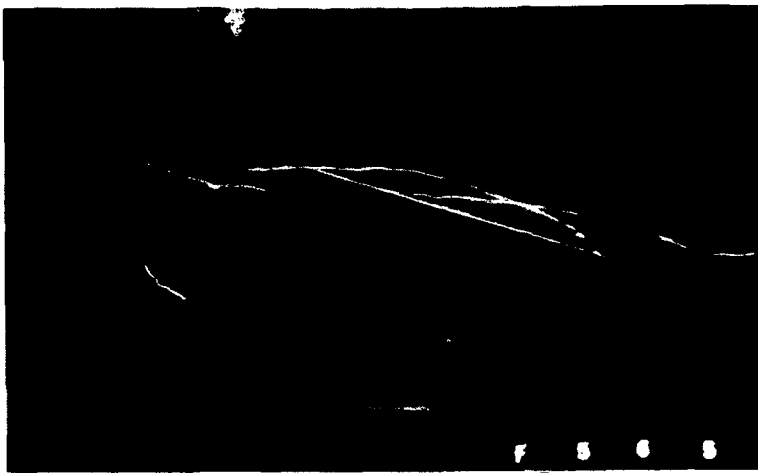


$1/c = 0.1$



$1/c = 0.2$

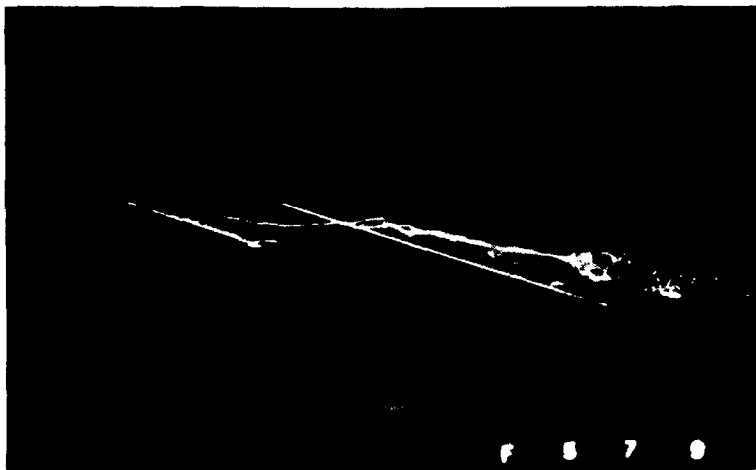
Fig.20 (contd.) Effect of canard longitudinal position on vortex
flow over low canard configuration (Plan view)
(Angle of attack = 18° , $h/c = -0.1$)



$1/c = -0.2$



$1/c = -0.1$



$1/c = 0$

Fig.21 Effect of canard longitudinal position on vortex flow over low canard configuration (Side view)
(Angle of attack = 18° , $h/c = -0.1$)



$1/c = 0.1$



$1/c = 0.2$

Fig.21 (contd.) Effect of canard longitudinal position on vortex
flow over low canard configuration (Side view)
(Angle of attack = 18° , $h/c = -0.1$)

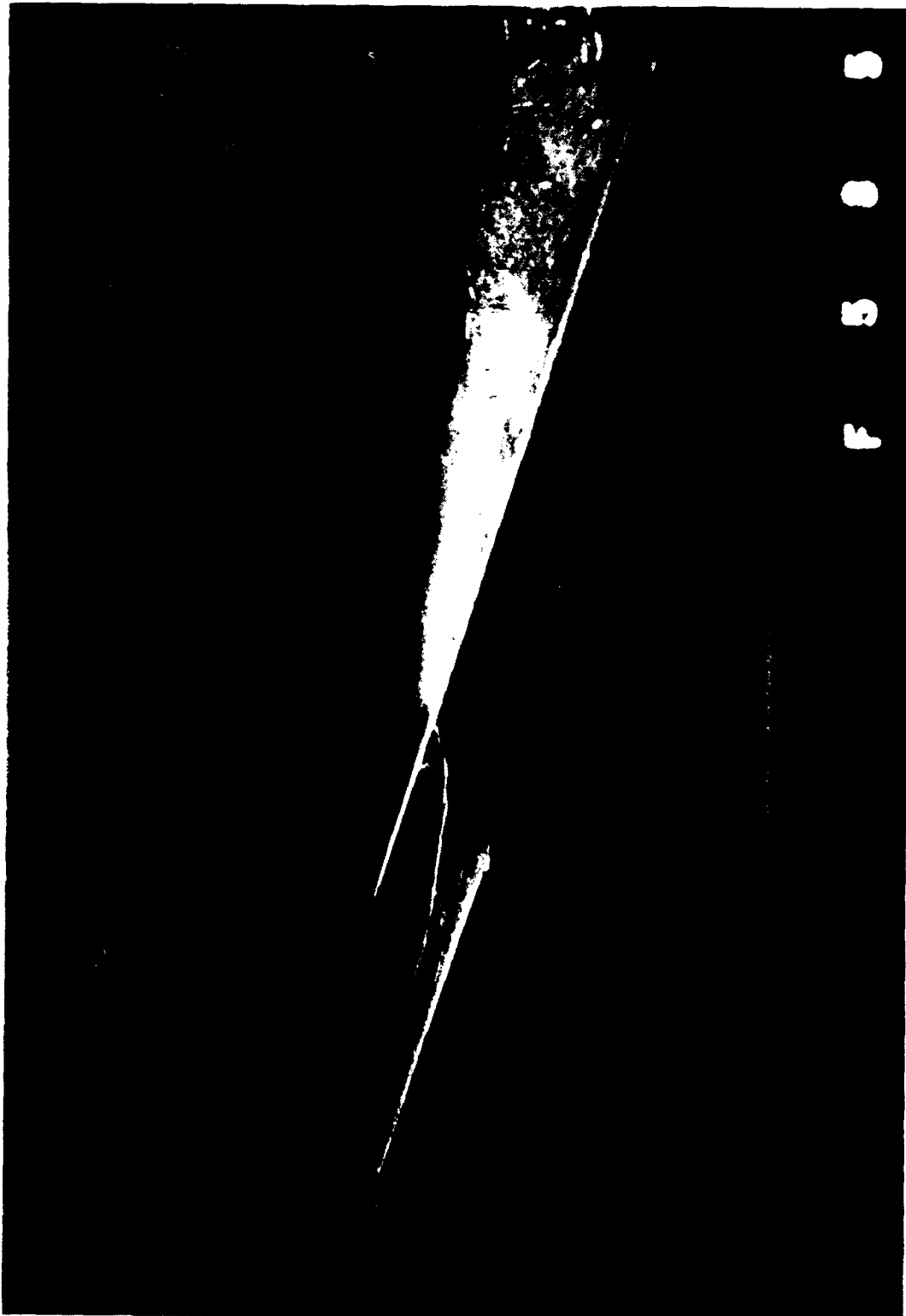
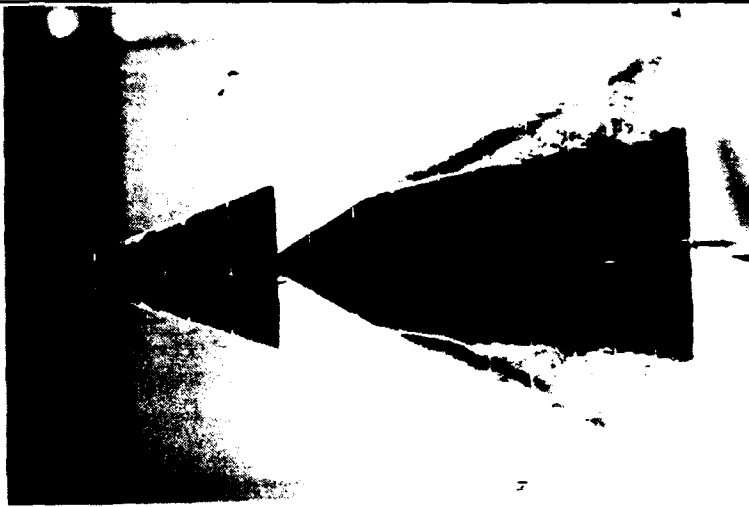
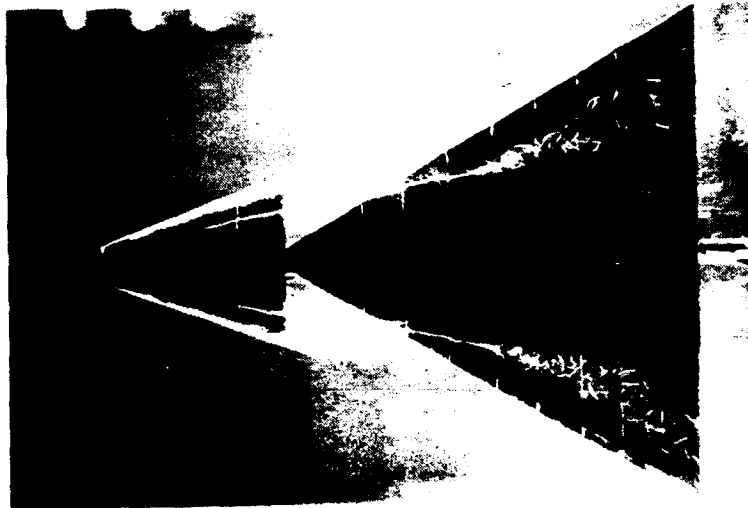


Fig.22 Canard vortex striking wing leading-edge
(Angle of attack = 18° , $h/c = -0.1$, $l/c = 0.08$)



Wing cathode only



Canard cathode only



Wing and canard cathodes

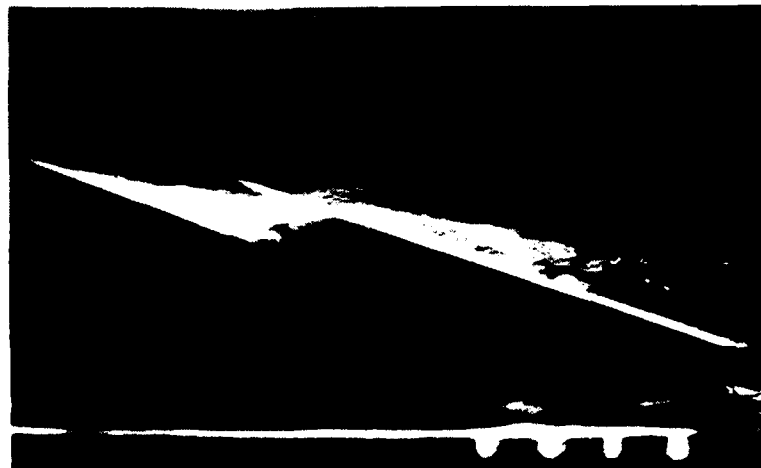
Fig.23 Use of separate canard and wing cathodes to visualise flow over low canard configuration (Plan view)
(Angle of attack = 18° , $h/c = -0.1$, $l/c = 0.05$)



Wing cathode only

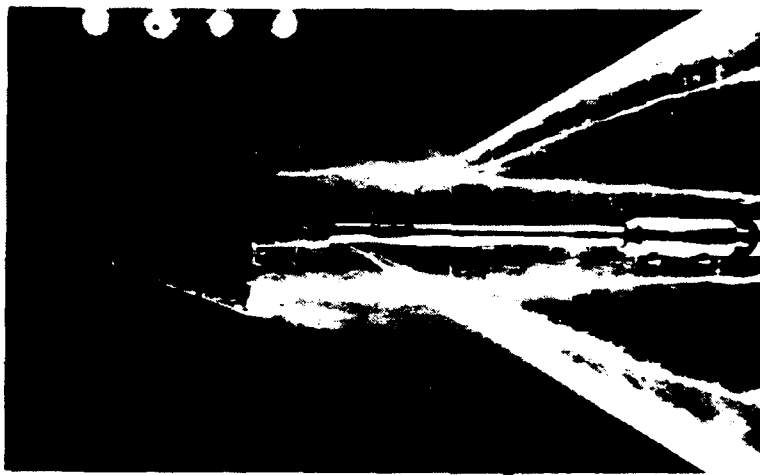


Canard cathode only

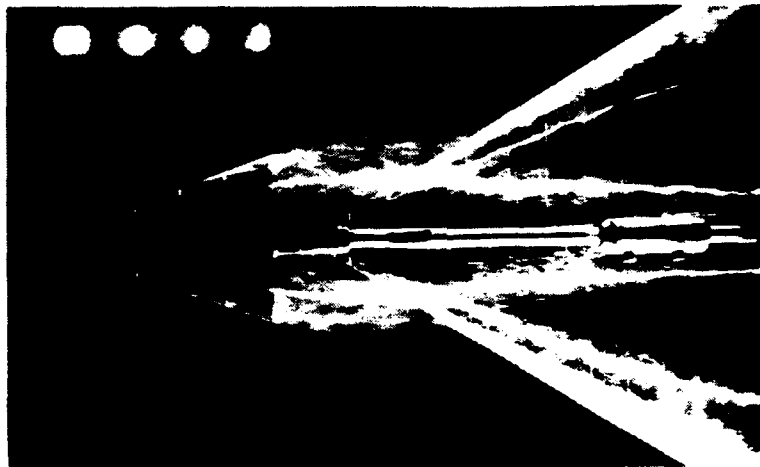


Wing and canard cathodes

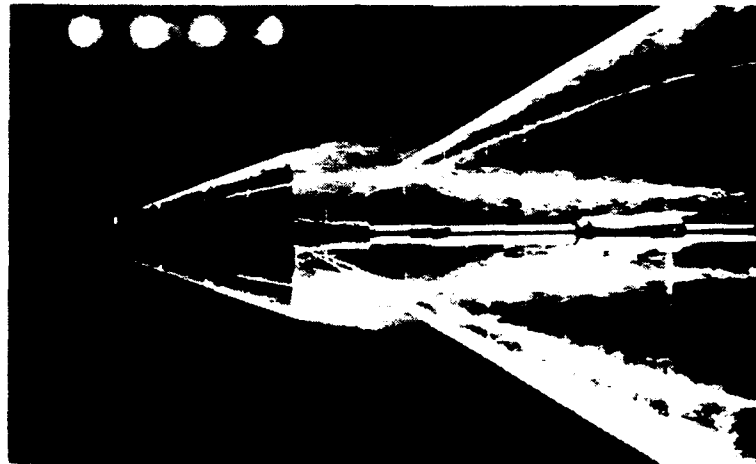
Fig.24 Use of separate canard and wing cathodes to visualise flow over low canard configuration (Side view)
(Angle of attack = 18° , $h/c = -0.1$, $l/c = 0.05$)



$$1/c = -0.2$$

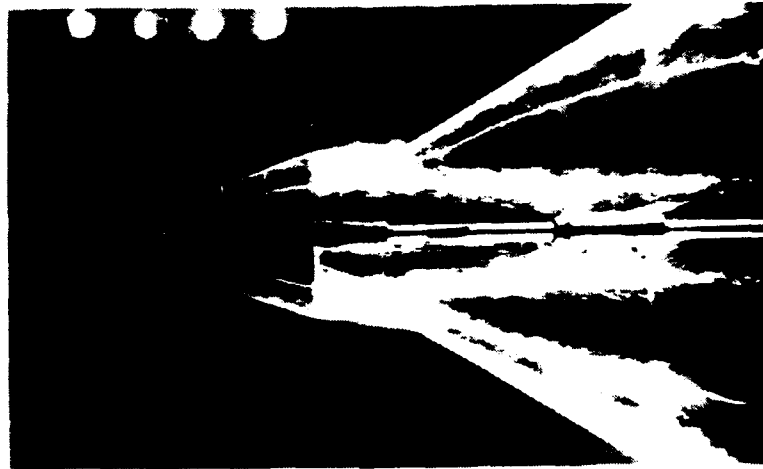


$$1/c = -0.1$$

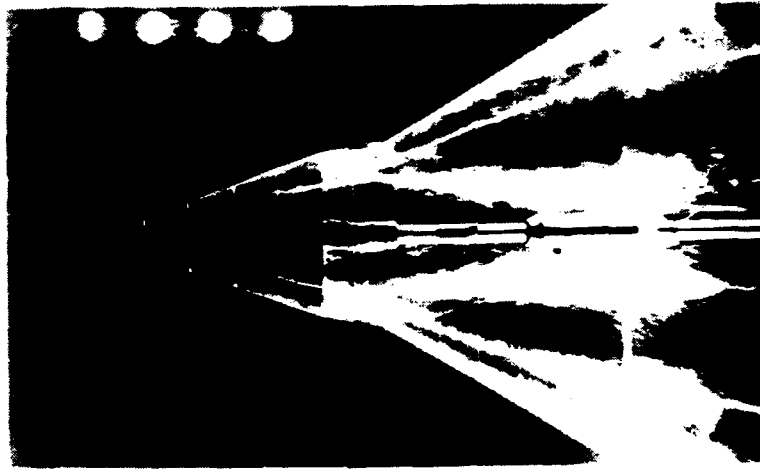


$$1/c = 0$$

Fig.25 Effect of canard longitudinal position on vortex flow over high canard configuration (Plan view)
(Angle of attack = 18° , $h/c = 0.1$)

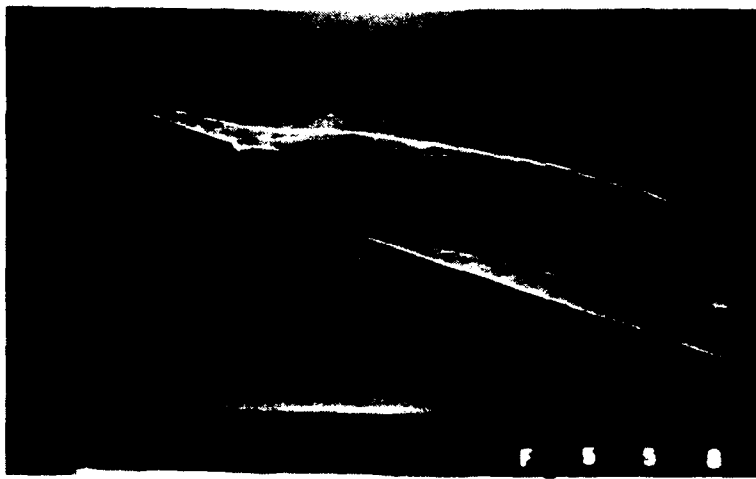


$1/c = 0.1$



$1/c = 0.2$

Fig.25 (contd.) Effect of canard longitudinal position on vortex flow over high canard configuration (Plan view)
(Angle of attack = 18° , $h/c = 0.1$)



$$1/c = -0.2$$



$$1/c = -0.1$$



$$1/c = 0$$

Fig.26 Effect of canard longitudinal position on vortex flow over high canard configuration (Side view)
(Angle of attack = 18° , $h/c = 0.1$)

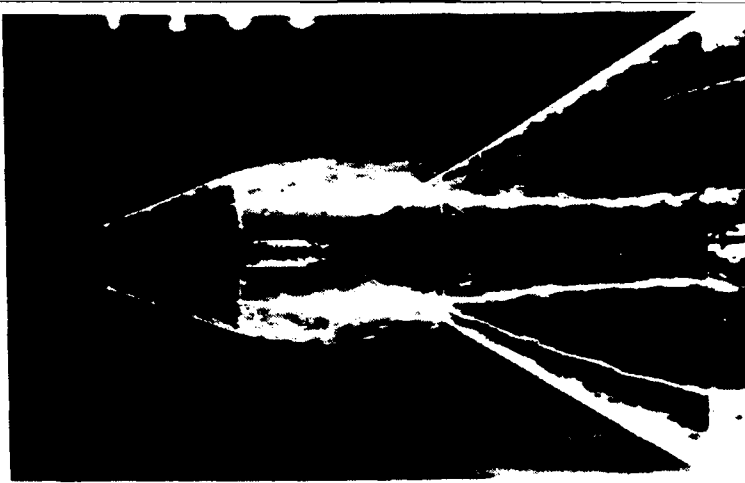


$1/c = 0.1$

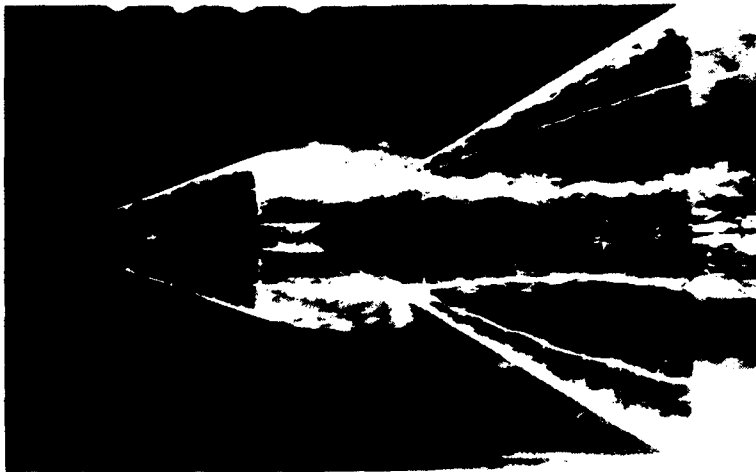


$1/c = 0.2$

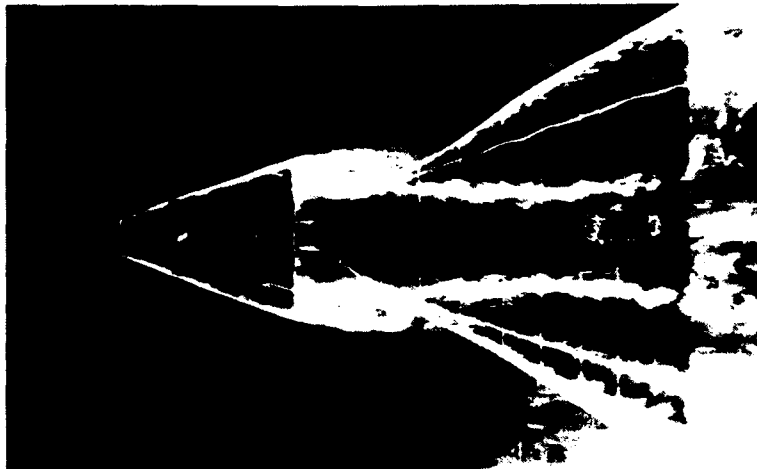
Fig.26 (contd.) Effect of canard longitudinal position on vortex flow over high canard configuration (Side view)
(Angle of attack = 18° , $h/c = 0.1$)



$$1/c = -0.2$$

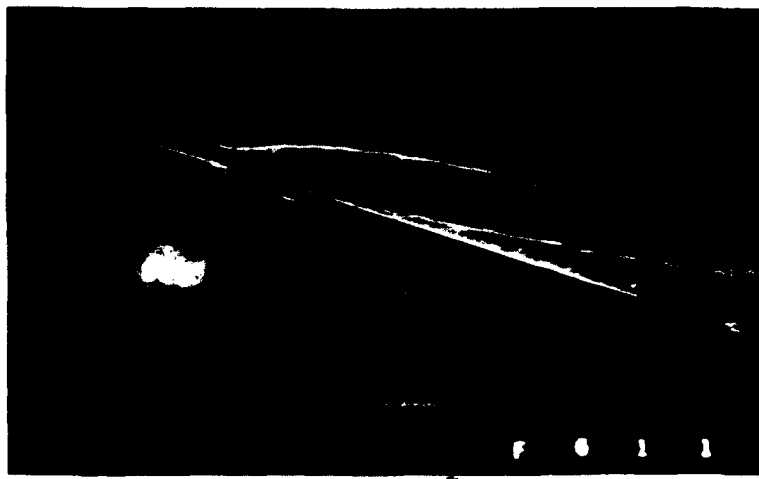


$$1/c = -0.1$$



$$1/c = 0$$

Fig.27 Effect of canard longitudinal position on vortex flow over mid-canard configuration (Plan view)
(Angle of attack = 18° , $h/c = 0$)



$1/c = -0.2$

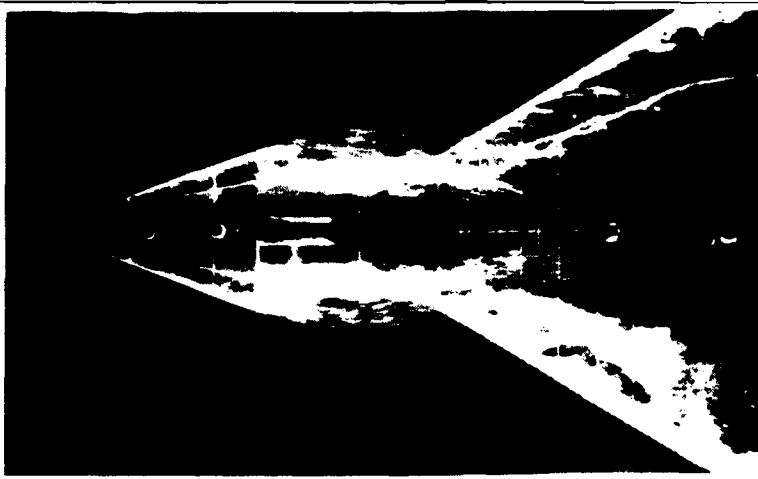


$1/c = -0.1$

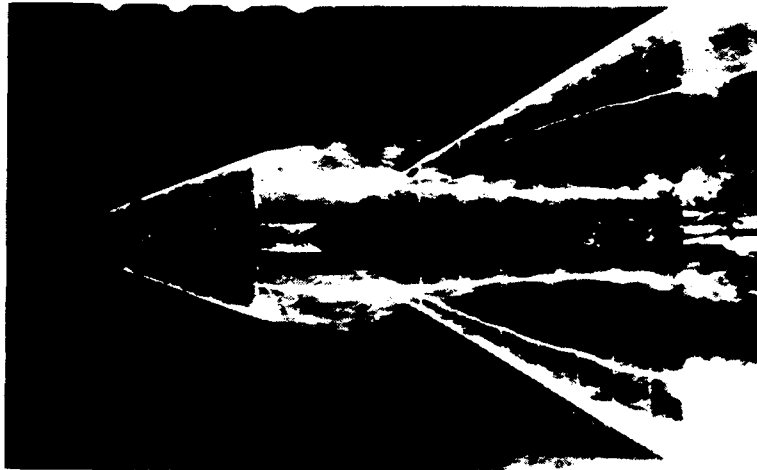


$1/c = 0$

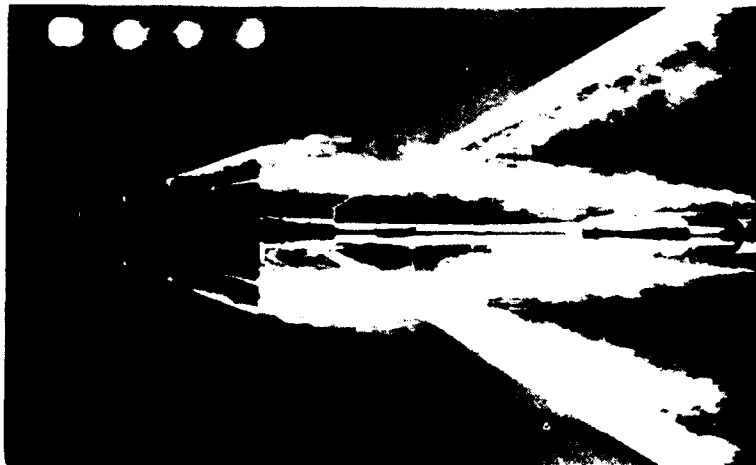
Fig.28 Effect of canard longitudinal position on vortex flow over mid-canard configuration (Side view)
(Angle of attack = 18° , $h/c = 0$)



$h/c = -0.1$

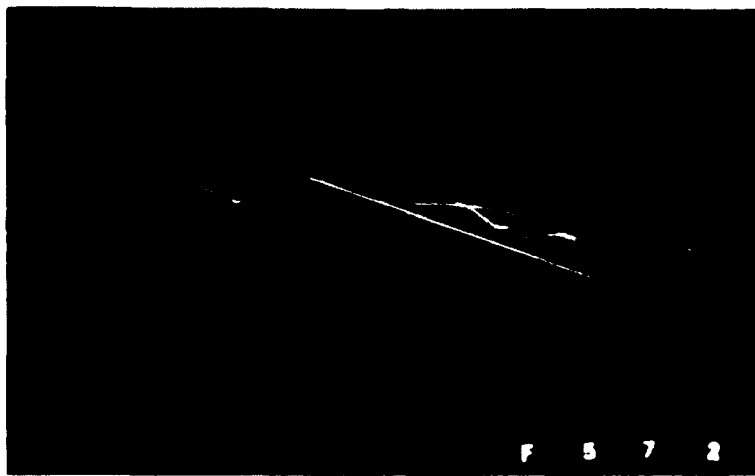


$h/c = 0$

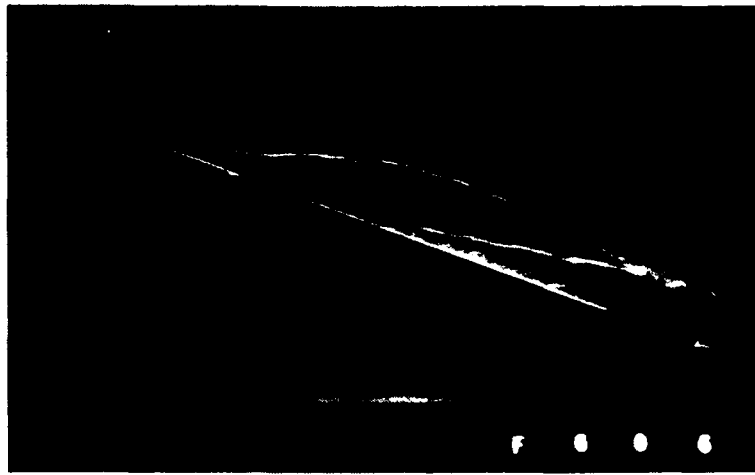


$h/c = 0.1$

Fig.29 Effect of canard vertical position on vortex flow over forward canard configuration (Plan view)
(Angle of attack = 20° , $1/c = -0.1$)



2
 $h/c = -0.1$

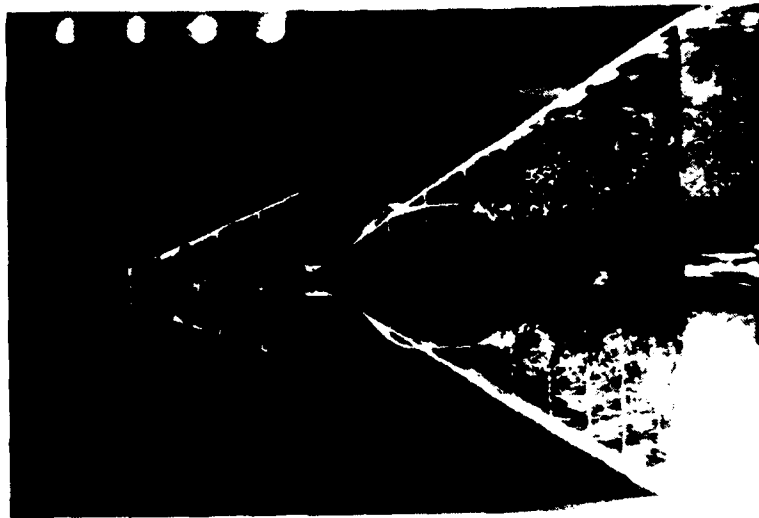


$h/c = 0$

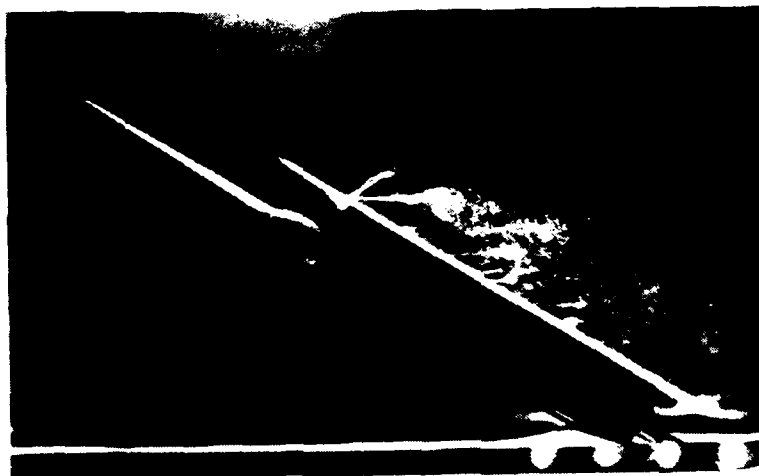


$h/c = 0.1$

Fig.30 Effect of canard vertical position on vortex flow over forward canard configuration (Side view)
(Angle of attack = 20° , $1/c = -0.1$)



(a) Plan view



(b) Side view

Fig.31 Vortex under wing apex, low canard configuration
(Angle of attack = 30° , $h/c = -0.1$, $l/c = 0.05$)



(a) $R = 5.2 \times 10^4$



(b) $R = 9.3 \times 10^4$

Fig.32 Close-up of vortex under wing apex, low canard configuration
(Side view)
(Angle of attack = 30° , $h/c = -0.1$, $1/c = 0.05$)



Fig.33 Perspective view of vortex under wing apex
(Angle of attack = 30° , $h/c = -0.1$, $1/c = 0.05$)



Fig.34 Video frame of vortex under wing apex, including canard
vortex and wing vortex (Side view)
(Angle of attack = 30° , $h/c = -0.1$, $l/c = 0.05$)

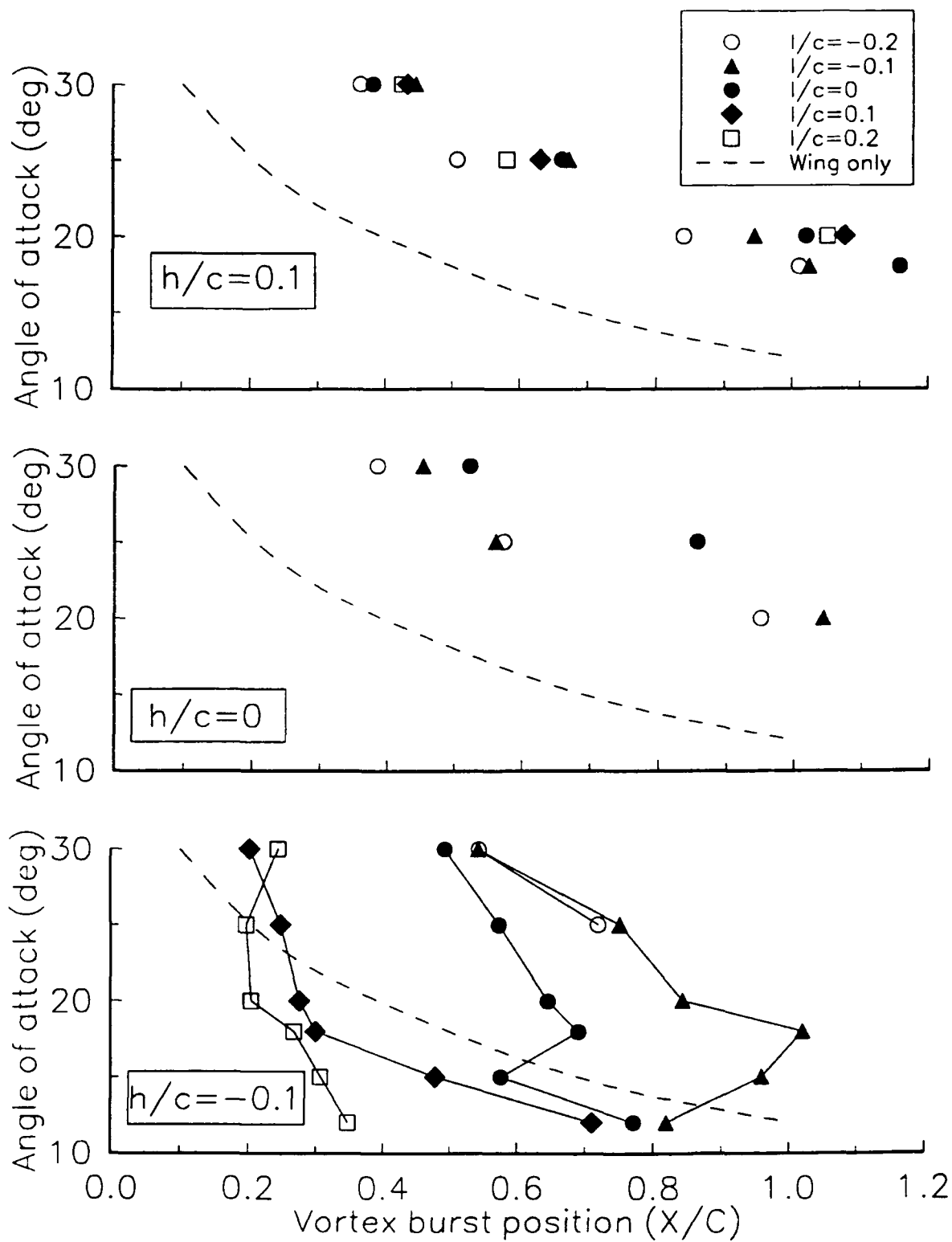
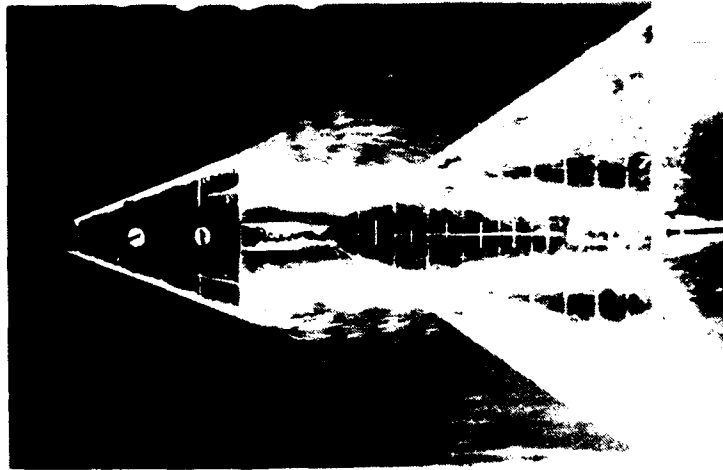
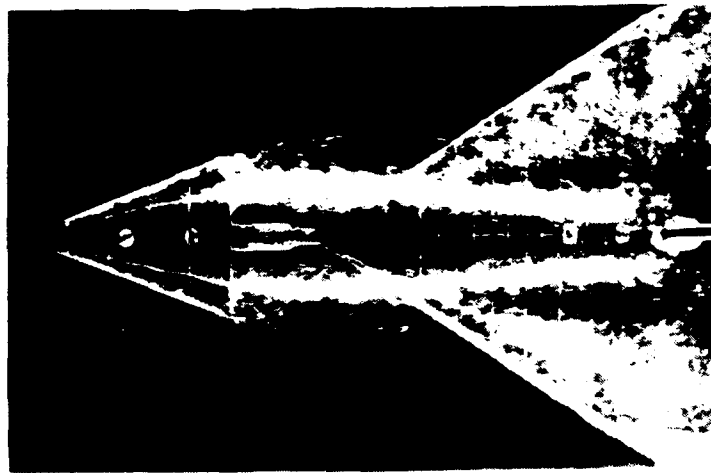


Fig.35 Effect of canard position on wing vortex breakdown position
 (Solid lines show results for 60° delta alone)



(a) $R = 9.6 \times 10^4$



(b) $R = 4.5 \times 10^4$

Fig.36 Bursting and reforming of mid-canard vortices in wing
flowfield (Plan view)
(Angle of attack = 30° , $h/c = 0$, $l/c = -0.2$)

Monash
Hargrave Library

Sydney
Engineering Library

Newcastle
Library

NSW
Physical Sciences Library

RMIT
Library

CANADA

NRC National Aeronautical Establishment
Library

Universities and Colleges

Toronto
Institute for Aerospace Studies

FRANCE

ONERA
Library

INDIA

National Aeronautical Laboratory
Information Centre

JAPAN

National Aerospace Laboratory
Library

NETHERLANDS

National Aerospace Laboratory (NLR)
Library
Dr H.W.M. Hoeijmakers

Delft University of Technology
Mr N.G. Verhaagen, Dept. of Aerospace Engineering

SWEDEN

Aeronautical Research Institute
Library

DISTRIBUTION

AUSTRALIA

Department of Defence

Defence Central

Chief Defence Scientist)
AS, Science Corporate Management)shared copy
FAS Science Policy)
Director, Departmental Publications
Counsellor, Defence Science, London (Doc Data sheet only)
Counsellor, Defence Science, Washington (Doc Data sheet only)
Scientific Adviser, Defence Central
OIC TRS, Defence Central Library
Document Exchange Centre, DSTIC (8 copies)
Defence Intelligence Organisation
Librarian H Block, Victoria Barracks, Melb (Doc Data sheet only)

Aeronautical Research Laboratory

Director
Library
Chief, Flight Mechanics & Propulsion Division
Head, Flight Mechanics Branch
Branch File - Flight Mechanics
B.D. Fairlie, Flight Mechanics
C.A. Martin (8 copies for distribution to TTCP HTP-5)
Author: D.H. Thompson (10 copies)

Navy Office

Navy Scientific Adviser (3 copies Doc Data sheet only)

Army Office

Scientific Adviser - Army (Doc Data sheet only)

Air Force Office

Air Force Scientific Adviser
Aircraft Research and Development Unit
Scientific Flight Group
Library
RAAF Academy, Pt. Cook

Statutory and State Authorities and Industry

Aero-Space Technologies Australia, Systems Division Librarian
ASTA Engineering, Document Control Office
Hawker de Havilland Aust Pty Ltd, Victoria, Library

Universities and Colleges

Melbourne
Engineering Library

UNITED KINGDOM

CAARC, Secretary
Defence Research Agency
Bedford, Library
Farnborough, Library
Mr J.H.B. Smith

Aircraft Research Association
Library

British Aerospace (Warton)
Library

Universities and Colleges

Bristol
Engineering Library
Professor M.V. Lowson
Dept. of Aerospace

Cambridge
Library, Engineering Department

Southampton
Library

Cranfield Inst. of Technology
Library

Imperial College
Aeronautics Library

UNITED STATES OF AMERICA

NASA Scientific and Technical Information Facility

NASA Ames Research Center
Mr L.B. Schiff
Fluid Mechanics Lab
Dr B.G. McLachlan

NASA Langley Research Center
Mr J.R. Chambers
Mr W.L. Sellers
Mr G.E. Erickson
Mr J.E. Lamar

Eidetics International
Mr G.N. Malcolm

Vigyan Research Associates Inc.
Dr D.M. Rao

PAGE CLASSIFICATION
UNCLASSIFIED

PRIVACY MARKING

THIS PAGE IS TO BE USED TO RECORD INFORMATION WHICH IS REQUIRED BY THE ESTABLISHMENT FOR ITS OWN USE BUT WHICH WILL NOT BE ADDED TO THE DISTIS DATA UNLESS SPECIFICALLY REQUESTED.

16. ABSTRACT (CONT).

17. IMPRINT

AERONAUTICAL RESEARCH LABORATORY, MELBOURNE

18. DOCUMENT SERIES AND NUMBER

Flight Mechanics Report 189

19. COST CODE

54 511F

20. TYPE OF REPORT AND PERIOD COVERED

21. COMPUTER PROGRAMS USED

22. ESTABLISHMENT FILE REF.(S)

23. ADDITIONAL INFORMATION (AS REQUIRED)